sciendo

CAIM
ISSN 2038-0909

Commun. Appl. Ind. Math. 16 (1), 2025, 41–61

DOI: 10.2478/caim-2025-0003

Research Article

Modelling and simulation of bread leavening to monitor energy consumption in industrial processes

Laura Rinaldi[1], Giulio G. Giusteri[1*]

[1]Dipartimento di Matematica "Tullio Levi-Civita", Università degli Studi di Padova, via Trieste 63, 35121, Padova, Italy

[*]Email address for correspondence: giulio.giusteri@unipd.it

Communicated by Antonio Cazzani
Received on 06 28, 2024. Accepted on 05 04, 2025.

Abstract

We introduce a mathematical model of bread leavening in a warm chamber by coupling heat transfer, yeast growth, and carbon dioxide production and diffusion with the deformation of baking paste. We analyze the corresponding system of partial differential equations. The system is discretized by using a semi-implicit Euler method and the finite-element method in the time and space domain, respectively. Numerical simulations are employed to identify the energy consumption necessary to achieve a target volume under different settings of the leavening chamber and different concentrations of yeast in the baking paste, thereby providing a tool for the identification of cost-effective protocols.

Keywords: Bread leavening, heat transfer and diffusion, finite elasticity with growth, coupled partial differential equations, energy consumption

AMS subject classification: 74F05, 80A20, 80M10, 35K51

1 Introduction

Bread is closely related to people's daily life and its making is an important operation in food industry. This is a complex process that involves physical, chemical and biochemical changes. Bread making can be divided into two sub-processes: the leavening and the baking. The leavening happens in a warm chamber and its result is a dough increased in volume due to the metabolic effect of yeast. The baking takes place in a hot oven that cooks the dough properly, making it a soft crumb inside and crunchy outside.

Nowadays, bread production is responsible for significant energy usage and CO_2 emission. To optimize the process and the energy consumption a lot of effort focuses on the cooking process in the oven [1–3]. Nevertheless, leavening is a much longer process and energy is spent both to accelerate leavening with heat and to slow it down by cooling. Issues of formulation, natural leavening time, rhythm of production, and final quality of the product influence with competing interests the use of energy in the bread making process.

The various phases of this process can be studied from different points of view. Many models focus their attention on the baking process, by developing partial differential equations to describe heat and mass transfer of different components and the overall energy balance [2,4–8]. Some works do not consider the volumetric expansion but only address the effects of cooking on the dough [1,4,5]. The leavening process is mostly treated by looking at chemical reactions [9] or by analyzing the effect of different amounts of wheat bran present in the dough [10], or from a microscale point of view through an analysis of CO_2 bubbles [9,11–13].

The aim of this work is to provide a mathematical model for bread leavening and to show how this can be used to monitor energy consumption in different scenarios. Such a model can form the basis for the development of digital twins for leavening chambers to achieve a more cost-effective and sustainable bread making process [14] and can be the starting point for the process optimization, as well as a way to facilitate product development as shown in [15].

Even though the technological sectors (automotive or aerospace industries) have made significant advances in applying process virtualization and optimal design, the food industry has still not fully exploited these benefits [16]. Novel ways of reducing energy consumption and food waste in the private, industrial, and public sectors while preserving or improving food quality are also needed [17]. Food industry is challenged for sustainability, to become energy- and process-efficient and reduce waste with top priority of safety and quality. The 'digitalization' of the agrifood sector is a diverse theme of current interest [18]. It is within this context that we developed our work.

For the sake of definiteness, we chose paradigmatic conditions as regards the geometry of the bread, corresponding to common industrial bread production. Nevertheless, our model is sufficiently flexible to be applied to more general conditions. We address the coupling of thermal conduction with the metabolism of yeast and with the consequent growth of the dough, which in turns affects the elastic properties of the material. All these effects contribute to the volume change observed during the leavening process. We develop a model that features a coupled system of ordinary and partial differential equations. These are solved numerically in a three-dimensional geometry and the results of the simulations are used to support the identification of optimal conditions to contain the energy consumption while achieving the desired target volume.

A finite-element computational model for bread leavening will be presented where the partial differential equations that describe heat exchange and the presence of yeast and carbon dioxide are coupled with the quasi-static deformation of the growing dough, justified by the very fast damping of elastic waves. In fact, the dough is treated as a hyperelastic material that acquires an equilibrium configuration under the action of its weight. The presence of yeast generates a volume expansion by producing carbon dioxide. From the mathematical point of view, this affects the relaxed configuration of the elastic body and induces growth. The leavening chamber operates approximately between 20°C and 50°C. The yeast concentration is initially assumed to be uniform in the dough, but the heating process creates non-uniform conditions for the production of CO_2 and hence for the leavening.

In Section 2, we define a continuum mechanical model that takes into account the elasticity and growth of the dough coupled to heat transfer, yeast growth, and carbon dioxide production and diffusion. In Section 3, we define the weak formulation of the differential problem and we prove uniqueness of solutions. The discretization scheme is presented in Section 4 and its convergence is used to prove the existence of weak solutions. Finally, in Section 5 we describe the implementation of the model and we carry out a sensitivity analysis to identify the energy necessary to achieve a target volume in different scenarios. We summarize our results and mention further research directions in Section 6.

2 Formulation of the model

The baking paste is mainly composed by flour and water, with the important presence of yeast and carbon dioxide as main players of the leavening process. We wish to model a situation in which the material grows within a baking tray (typically made of steel) that constrains the lateral volume growth while allowing for vertical expansion.

The *material domain* $\Omega_\mathrm{b} \subset \mathbb{R}^3$ provides a fixed set of labels for the material points of the dough. The actual space occupied by the material is given by $\boldsymbol{u}(\Omega_\mathrm{b})$, where $\boldsymbol{u} : \Omega_\mathrm{b} \to \mathbb{R}^3$ is the deformation map. We partition the boundary of Ω_b as the disjoint union of three parts: Γ_0 identifies the points that are in contact with the bottom side of the baking tray, Γ_1 the top points in contact with air, and Γ_2 the material points in contact with the lateral sides of the tray. The different quantities involved in the description of the process are represented by fields on the fixed material domain Ω_b. A list of symbols is given in Table 1.

2.1 Elasticity of the bread

To determine the actual shape of the dough under given conditions, we model it as a hyperelastic material of neo-Hookean type [19]. We denote by F the deformation gradient and set $J := \det \mathsf{F}$. Over time, the dough will expand and, to model this, we need to introduce the dilation field $J_\mathrm{ref} : \Omega_\mathrm{b} \to \mathbb{R}^+$

Table 1. List of symbols.

Functions	
$\boldsymbol{u}$	deformation
θ	temperature
D	concentration of CO_2
Y	yeast concentration
K_{y}	yeast growth rate function
f	CO_2 production rate function
Constants	
λ and μ	Lamé's moduli
E	Young's modulus
ν	Poisson's ratio
$\boldsymbol{B}$	body force
k	thermal conductibility
h	heat transfer coefficient
c	specific heat
ρ	density
β	diffusivity
n_{mol}	the number of moles contained in a gram of CO_2
Subscripts	
0	initial condition
b	baking paste
f	flour
o	outside, leavening machine
w	water
t	steel tray
y	yeast
CO_2	carbon dioxide
bo	bread-to-air
bt	bread-to-tray

that describes, locally, the target volume that the material would like to achieve in the absence of any constraint. Notice that this target volume is the result of the competition between the expansion generated by the presence of carbon dioxide bubbles end the resistance of the baking paste. We assume that the production of carbon dioxide by the yeast is sufficiently slow that an equilibrium between the different pressures is rapidly achieved. We thus summarize the detailed processes involved in the expansion in the quasistatic evolution of J_{ref}.

By introducing the right Cauchy–Green tensor $\mathbf{C}$ and a body force per unit volume $\boldsymbol{B}$, that will represent the weight, the elastic energy functional is postulated to be

$$\mathcal{E}(\boldsymbol{u}) = \frac{1}{2}\int_{\Omega_{\mathrm{b}}} \left[\mu\left(\operatorname{tr}\mathbf{C} - 3J_{\mathrm{ref}}^{2/3}\right) + \lambda|\log(J/J_{\mathrm{ref}})|^2\right] d\boldsymbol{X} - \int_{\Omega_{\mathrm{b}}} \boldsymbol{B}\cdot\boldsymbol{u}\, d\boldsymbol{X}, \tag{1}$$

where λ and μ are the usual Lamé's moduli

$$\mu = \frac{E}{2(1+\nu)}, \qquad \lambda = \frac{E\nu}{(1+\nu)(1-2\nu)}, \tag{2}$$

with E the Young modulus and ν the Poisson ratio. These material parameters may depend on temperature, but we will neglect this feature since we are dealing with a small temperature range. There will be an indirect dependence of E on temperature, because the Young modulus will change with the evolution of carbon dioxide, which in turn is affected by temperature.

In the analysis of the leavening process, it is reasonable to neglect vibrations of the dough, because inertial phenomena linked to the elastic response take place on a much faster timescale than heat transfer, diffusion processes, and volume growth, and the mechanical dissipation dampens vibrations quite fast. We then follow the deformation of the material with a quasi-static approach. The fact that we are assuming a strong dissipation with a quasi-static evolution justifies that constitutive choice of neo-Hookean type.

Indeedd, a more precise rheological model for the baking paste would be of viscoelastic type, featuring dissipation and stress relaxation, but in the quasi-static approach, we do not need to specify the viscous stress. Similarly, the stress relaxation that follows expansion is implicitly described by the evolution of the parameter J_{ref} given below.

At each time, the deformation map $\boldsymbol{u}$ is obtained by solving the Euler–Lagrange equation $\delta\mathcal{E}(\boldsymbol{u}) = 0$, subject to the following boundary conditions:

$$\boldsymbol{u} = (0,0,0) \qquad \text{on } \Gamma_0, \tag{3}$$

$$\boldsymbol{u} = (0,0,u_z) \qquad \text{on } \Gamma_2, \tag{4}$$

where the last condition means that the only displacement allowed on Γ_2 is along the z-direction. This sliding condition on u_z is complemented by the natural traction-free boundary condition, since we neglect friction between the dough and the walls.

These imply that the material points are fixed at the bottom, while they can slide vertically along the lateral sides of the tray. Lastly, on the free surface Γ_1 we have a traction-free condition, also known as natural boundary condition, emerging from the variational problem of energy minimization. The equation for the deformation map is coupled with evolution equations for other quantities, introduced below, via the dependence of the target volume J_{ref} and the Young modulus E on the concentration of carbon dioxide, which, in turn, depends on the yeast activity and the temperature field.

2.2 Heat transfer

The second equation considered in the model is the heat equation, that describes the temperature evolution of the dough during leavening. Whereas heat fluxes are more easily described in the context of spatial domains in the actual configuration of the material, for the sake of simplicity of the numerical solution of the equations, we prefer to work with the fixed domain Ω_{b} for all of the fields involved in the model. We then need to rewrite the classical heat equation for a homogeneous domain in material coordinates. The details of this procedure are given in Appendix A.

We consider the evolution over a fixed time interval $[0,\tau]$ of the temperature field $\theta_{\mathrm{b}} : \Omega_{\mathrm{b}} \times [0,\tau] \to \mathbb{R}$ as given by the equation

$$\rho_{\mathrm{b}} c_{\mathrm{b}} J \frac{\partial \theta_{\mathrm{b}}}{\partial t} = \operatorname{div}(\beta_{\mathrm{b}} J \mathbf{C}^{-1} \nabla \theta_{\mathrm{b}}) \qquad \text{on } \Omega_{\mathrm{b}} \times [0,\tau], \tag{5}$$

where ρ_{b} is the density of the baking paste, c_{b} the specific heat and β_{b} is the thermal conductivity. It is worth noticing that the isotropic and homogeneous diffusion that takes place in spatial coordinates becomes anisotropic and non-homogeneous in material coordinates, as is evident from the presence of the term $J\mathbf{C}^{-1}$ in the heat flux. For this equation, we need to prescribe initial conditions and we add boundary conditions (of Robin type) describing the energy exchanged between the bread and the air in the leavening chamber. We set $\Gamma_3 := \Gamma_0 \cup \Gamma_2$ to represent the portion of the boundary that is in contact with the baking tray. We do not resolve the heat flow within the tray, but simply summarize its effect in the transfer coefficient h_{bt} which is different from the one describing the direct transfer of heat between air and bread, namely h_{bo}. Denoting by $\boldsymbol{m}$ the unit outer normal to $\partial\Omega_{\mathrm{b}}$, the boundary and initial conditions for the temperature field read

$$\theta_{\mathrm{b}}(\cdot,0) = \theta_{\mathrm{b}_0} \qquad \text{on } \Omega_{\mathrm{b}}, \tag{6}$$

$$-\beta_{\mathrm{b}} J(\mathbf{C}^{-1}\nabla\theta_{\mathrm{b}}) \cdot \boldsymbol{m} = |J\mathbf{F}^{-\mathsf{T}}\boldsymbol{m}| h_{\mathrm{bt}}(\theta_{\mathrm{b}} - \theta_{\mathrm{o}}) \qquad \text{on } \Gamma_3 \times [0,\tau], \tag{7}$$

$$-\beta_{\mathrm{b}} J(\mathbf{C}^{-1}\nabla\theta_{\mathrm{b}}) \cdot \boldsymbol{m} = |J\mathbf{F}^{-\mathsf{T}}\boldsymbol{m}| h_{\mathrm{bo}}(\theta_{\mathrm{b}} - \theta_{o}) \qquad \text{on } \Gamma_1 \times [0,\tau]. \tag{8}$$

Notice that we assume the tray temperature equal to the one of the surrounding air θ_o since the tray thermalizes much faster than the baking paste.

2.3 Yeast growth

A key role in the leavening is played by the presence and metabolism of yeast. The function $Y : \Omega_b \times [0,\tau] \to \mathbb{R}^+$ represents the concentration of yeast in the dough with respect to the flour quantity, that we suppose to be uniform at the initial time. Given an initial condition Y_0, the yeast concentration evolves according to the Cauchy problem [9,12,13]

$$\begin{cases} \frac{d}{dt}Y = K_y(\theta_b)Y & \text{on } \Omega_b \times [0,\tau], \\ Y(\cdot,0) = Y_0 & \text{on } \Omega_b, \end{cases} \tag{9}$$

where K_y is the growth rate function modeled as a cubic polynomial (Figure 1(a)) that vanishes at 0°C and at the yeast death temperature θ_y:

$$K_y(\theta) := \max\left\{\lambda_y \frac{27\,\theta^2(\theta_y - \theta)}{4\,\theta_y^3}, K_{\min}\right\}, \tag{10}$$

where $K_{\min} := \lambda_y \frac{27\,60^2(\theta_y - 60)}{4\,\theta_y^3}$. We modeled the function K_y by supposing that yeasts live in a temperature range between 0°C and θ_y therefore, below a certain temperature there is no activity and above another temperature they die. Moreover, they produce CO_2 due to their metabolic activity only when the temperature is greater than 5°C. A typical value for θ_y is 50°C, while the constant λ_y of unit s^{-1} is calibrated following Ref. [10]. Specifically, we chose its value in such a way that the volume expansion obtained in our simulations is comparable with the one reported in Ref. [10].

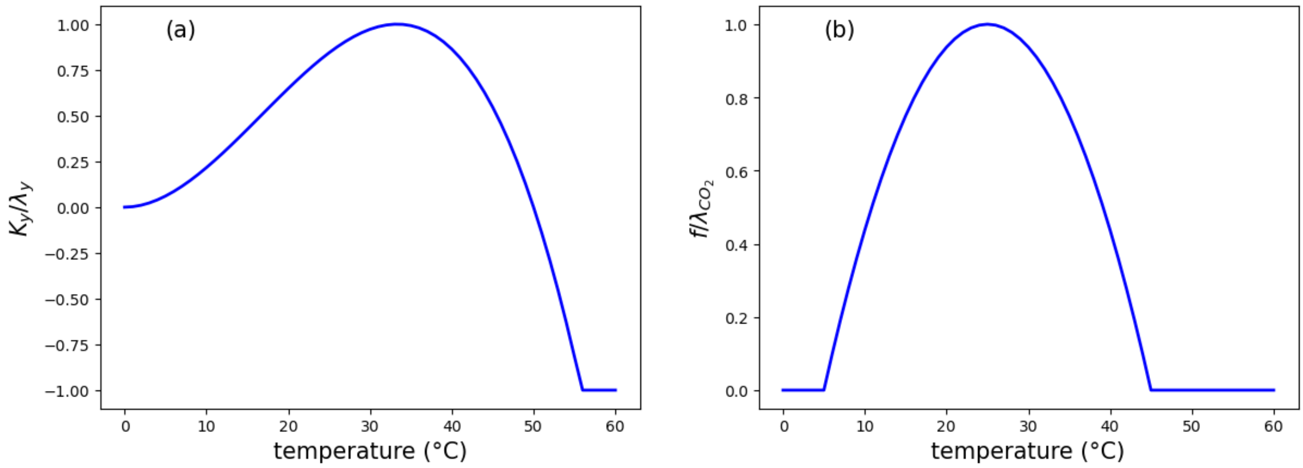

Figure 1. (a) The normalized growth rate function K_y/λ_y as a function of the temperature. (b) The normalized CO_2 production rate f/λ_{CO_2} as a function of temperature.

2.4 Production and diffusion of carbon dioxide

The metabolism of yeast involves the production of carbon dioxide. The CO_2 concentration with respect to flour, denoted by $D : \Omega_b \times [0,\tau] \to \mathbb{R}$, has a diffusive evolution with a source term depending on the rate of CO_2 production f, on the temperature reached by the bread θ_b and on the yeast concentration Y. The equation for D is then

$$J\frac{\partial D}{\partial t} = \operatorname{div}(\beta_{CO_2} J \mathbf{C}^{-1}\nabla D) + J\,f(\theta_b)Y \qquad \text{on } \Omega_b \times [0,\tau], \tag{11}$$

$$D(\cdot,0) = D_0 \qquad \text{on } \Omega_b. \tag{12}$$

The boundary condition is of homogeneous Neumann type and the CO_2 production rate $f(\theta)$ is modeled by

$$f(\theta) := \max\left\{0, \lambda_{CO_2}\frac{(\theta-\theta_{\text{low}})(\theta_{\text{high}}-\theta)}{\zeta}\right\}, \tag{13}$$

with λ_{CO_2} a constant rate of units s^{-1}, $\theta_{\text{low}} = 5°\text{C}$ and $\theta_{\text{high}} = 45°\text{C}$ the limits of the temperature range in which there is production, and $\zeta = 400°\text{C}^2$ is a normalization constant (see Figure 1(b)). More precisely, $f(\theta_{\text{b}})$ expresses the temperature-dependent rate of CO_2 produced per unit of yeast concentration, thus the total amount of CO_2 produced per unit time by yeast metabolism is given by $f(\theta_{\text{b}})Y$, which appears as a forcing term on the right-hand-side of (11).

2.5 Volume expansion

The carbon dioxide production due to fermentation implies a positive volume expansion associated with the leavening process. First of all, we introduce an estimate of the added CO_2 volume. For the sake of simplicity, we assume a linear relation between volume and temperature, by approximating the actual thermodynamic relation with the ideal gas law. At this stage, further corrections to that relation can be included in an empirical fitting coefficient. We thus compute the volume of the CO_2 gas considering the number of moles contained in a gram of CO_2, that is

$$PV^{1g}_{CO_2} = n_{\text{mol}}R\theta_{\text{b}}, \qquad V^{1g}_{CO_2} = \frac{n_{\text{mol}}R\theta_{\text{b}}}{P}, \tag{14}$$

where P is the pressure, n_{mol} is the number of moles contained in a gram of CO_2 and R is the ideal gas constant of units $\text{J}/\text{mol}\,\text{K}$. With this value, we can then update the dilation coefficient of the target volume configuration according to

$$J_{\text{ref}} = 1 + \frac{V^{1g}_{CO_2}DF_{\text{rate}}}{V^{1g}_0}, \tag{15}$$

where V^{1g}_0 is the total volume of one gram of dough and F_{rate} the flour fraction of the paste.

At the same time, the Young modulus changes depending on the concentration of CO_2. If we assume that the Young modulus E_{CO_2} of CO_2 is negligible compared to that of the dough, we can argue that its presence weakens the elastic response. Denoting by E_0 the Young modulus of the dough at the initial time, we postulate that, locally, $E = E_0/J_{\text{ref}}$.

We stress that, in our model, while the target volume is determined by the updated value of J_{ref}, the actual volume expansion is obtained by minimizing the elastic energy (1), which depends on both the value of the target volume and the updated stiffness of the dough. The coupling with the temperature and CO_2 evolution is mediated by the updating of those parameters.

3 Weak form and uniqueness of the evolution

In this section we establish the uniqueness of solutions for the evolution equations concerning the temperature and CO_2 and yeast concentrations, under the assumption that a static deformation is given. To this end we need to introduce the weak form of the parabolic PDEs.

We introduce test functions $\tilde{\theta}_{\text{b}}$ for the heat equation and $\tilde{D}$ for the diffusion equation of carbon dioxide. The weak formulation of (5)–(8) and (11)–(12) is then

$$\begin{aligned}\int_0^\tau\int_{\Omega_{\text{b}}} \rho_{\text{b}}c_{\text{b}}\,J\frac{\partial\theta_{\text{b}}}{\partial t}\tilde{\theta}_{\text{b}}\,d\boldsymbol{X}\,dt + \int_0^\tau\int_{\Omega_{\text{b}}}(\beta_{\text{b}}\,J\,\mathbf{C}^{-1}\nabla\theta_{\text{b}})\cdot\nabla\tilde{\theta}_{\text{b}}\,d\boldsymbol{X}\,dt \\ = \int_0^\tau\int_{\Gamma_1} h_{\text{bo}}(\theta_o-\theta_{\text{b}})\tilde{\theta}_{\text{b}}|J\,\mathbf{F}^{-\mathsf{T}}\boldsymbol{m}|\,dS\,dt + \int_0^\tau\int_{\Gamma_3} h_{\text{bt}}(\theta_o-\theta_{\text{b}})\tilde{\theta}_{\text{b}}|J\,\mathbf{F}^{-\mathsf{T}}\boldsymbol{m}|\,dS\,dt\end{aligned} \tag{16}$$

and

$$\int_0^\tau \int_{\Omega_\mathrm{b}} J\,\frac{\partial D}{\partial t}\tilde{D}\,d\boldsymbol{X}\,dt + \int_0^\tau \int_{\Omega_\mathrm{b}} (\beta_{\mathrm{CO}_2}\,J\,\mathbf{C}^{-1}\nabla D)\cdot(\nabla\tilde{D})\,d\boldsymbol{X}\,dt = \int_0^\tau \int_{\Omega_\mathrm{b}} f(\theta_\mathrm{b})\,Y\,\tilde{D}J\;d\boldsymbol{X}\,dt. \tag{17}$$

Given that the deformation is fixed over the time interval $[0,\tau]$, in the next two sections we can assume the boundedness condition $J\mathbf{C}^{-1} \in L^\infty([0,\tau];L^\infty(\Omega_\mathrm{b}))$.

Theorem 3.1. *The continuum problem given by the equations (16)-(17) coupled with (9) has at most one solution with θ_b and D in $\in L^2([0,\tau];H^1(\Omega_\mathrm{b}))$ and $Y \in L^2([0,\tau];L^2(\Omega_\mathrm{b}))$, for any choice of the finite time interval $[0,\tau]$ and of initial conditions in $L^2(\Omega_\mathrm{b})$ for each field.*

Proof. Let us consider two weak solutions of our problem $g^{(1)}(\boldsymbol{X},t)$ and $g^{(2)}(\boldsymbol{X},t)$, with equal initial conditions, represented as vectors given by

$$g^{(1)}(\boldsymbol{X},t) = \begin{pmatrix}\theta_\mathrm{b}^{(1)}(\boldsymbol{X},t)\\ Y^{(1)}(\boldsymbol{X},t)\\ D^{(1)}(\boldsymbol{X},t)\end{pmatrix}, \qquad g^{(2)}(\boldsymbol{X},t) = \begin{pmatrix}\theta_\mathrm{b}^{(2)}(\boldsymbol{X},t)\\ Y^{(2)}(\boldsymbol{X},t)\\ D^{(2)}(\boldsymbol{X},t)\end{pmatrix}. \tag{18}$$

We wish to estimate the L^2-norm of the difference between the two solutions computed at time t, given by

$$\begin{aligned}\|g^{(1)}(\boldsymbol{X},t) - g^{(2)}(\boldsymbol{X},t)\|^2_{L^2(\Omega_\mathrm{b})} &= \|\theta_\mathrm{b}^{(1)}(\boldsymbol{X},t) - \theta_\mathrm{b}^{(2)}(\boldsymbol{X},t)\|^2_{L^2(\Omega_\mathrm{b})}\\ &\quad + \|Y^{(1)}(\boldsymbol{X},t) - Y^{(2)}(\boldsymbol{X},t)\|^2_{L^2(\Omega_\mathrm{b})} + \|D^{(1)}(\boldsymbol{X},t) - D^{(2)}(\boldsymbol{X},t)\|^2_{L^2(\Omega_\mathrm{b})}.\end{aligned} \tag{19}$$

Let us start with the weak solutions $\theta_\mathrm{b}^{(1)}, \theta_\mathrm{b}^{(2)}$ of equation (16). By taking the difference of the equations satisfied by the two solutions at a given time t we easily get

$$\begin{aligned}&\int_{\Omega_\mathrm{b}} \rho_\mathrm{b}\,c_\mathrm{b}\,J\frac{\partial(\theta_\mathrm{b}^{(1)} - \theta_\mathrm{b}^{(2)})}{\partial t}\tilde{\theta}_\mathrm{b}\,d\boldsymbol{X} + \int_{\Omega_\mathrm{b}} (\beta_\mathrm{b}\,J\,\mathbf{C}^{-1}\nabla(\theta_\mathrm{b}^{(1)} - \theta_\mathrm{b}^{(2)}))\cdot(\nabla\tilde{\theta}_\mathrm{b})\,d\boldsymbol{X}\\ &= \int_{\Gamma_1} h_\mathrm{bo}(\theta_\mathrm{b}^{(2)} - \theta_\mathrm{b}^{(1)})\tilde{\theta}_\mathrm{b}|J\,\mathbf{F}^{-\mathsf{T}}\boldsymbol{m}|\,dS + \int_{\Gamma_3} h_\mathrm{bt}(\theta_\mathrm{b}^{(2)} - \theta_\mathrm{b}^{(1)})\tilde{\theta}_\mathrm{b}|J\,\mathbf{F}^{-\mathsf{T}}\boldsymbol{m}|\,dS.\end{aligned} \tag{20}$$

By choosing $\tilde{\theta}_\mathrm{b} = (\theta_\mathrm{b}^{(1)} - \theta_\mathrm{b}^{(2)})$, we obtain

$$\begin{aligned}&\int_{\Omega_\mathrm{b}} \rho_\mathrm{b}\,c_\mathrm{b}\,J\frac{1}{2}\frac{\partial(\theta_\mathrm{b}^{(1)} - \theta_\mathrm{b}^{(2)})^2}{\partial t}\,d\boldsymbol{X} + \int_{\Omega_\mathrm{b}} \beta_\mathrm{b}\,J\,\mathbf{C}^{-1}\nabla(\theta_\mathrm{b}^{(1)} - \theta_\mathrm{b}^{(2)})\cdot\nabla(\theta_\mathrm{b}^{(1)} - \theta_\mathrm{b}^{(2)})\,d\boldsymbol{X}\\ &\qquad = -\int_{\Gamma_1} h_\mathrm{bo}(\theta_\mathrm{b}^{(1)} - \theta_\mathrm{b}^{(2)})^2|J\,\mathbf{F}^{-\mathsf{T}}\boldsymbol{m}|\,dS - \int_{\Gamma_3} h_\mathrm{bt}(\theta_\mathrm{b}^{(1)} - \theta_\mathrm{b}^{(2)})^2|J\,\mathbf{F}^{-\mathsf{T}}\boldsymbol{m}|\,dS,\end{aligned} \tag{21}$$

from which (see Appendix B) we conclude that

$$\frac{1}{2}\frac{d}{dt}\int_{\Omega_\mathrm{b}} \rho_\mathrm{b}\,c_\mathrm{b}\,J|\theta_\mathrm{b}^{(1)} - \theta_\mathrm{b}^{(2)}|^2\,d\boldsymbol{X} \le 0. \tag{22}$$

Finally, by integrating in time we obtain

$$\int_{\Omega_\mathrm{b}} \rho_\mathrm{b}\,c_\mathrm{b}\,J|\theta_\mathrm{b}^{(1)}(\boldsymbol{X},t) - \theta_\mathrm{b}^{(2)}(\boldsymbol{X},t)|^2\,d\boldsymbol{X} \le \int_{\Omega_\mathrm{b}} \rho_\mathrm{b}\,c_\mathrm{b}\,J|\theta_\mathrm{b}^{(1)}(\boldsymbol{X},0) - \theta_\mathrm{b}^{(2)}(\boldsymbol{X},0)|^2\,d\boldsymbol{X}. \tag{23}$$

We work under the assumption that $J(\boldsymbol{X}) \ge J_\mathrm{min} > 0$. Combining this with the equality of initial conditions, we get

$$\rho_\mathrm{b}c_\mathrm{b}\,J_\mathrm{min}\|\theta_\mathrm{b}^{(1)} - \theta_\mathrm{b}^{(2)}\|^2_{L^2(\Omega_\mathrm{b})} \le 0. \tag{24}$$

The previous formula tells us that $\|\theta_{\mathrm{b}}^{(1)} - \theta_{\mathrm{b}}^{(2)}\|_{L^2(\Omega_{\mathrm{b}})} = 0$ for each $t \in [0, \tau]$.

Given that the solution for the temperature field θ_{b} is unique and the function $K_{\mathrm{y}}(\theta_{\mathrm{b}})Y$ is continuous and Lipschitz in Y uniformly in t, there exists a unique solution Y for the Cauchy problem (9) for each fixed material point $\boldsymbol{X}$.

Finally by considering (17) and taking the difference between two solutions $D^{(1)}, D^{(2)}$ we get

$$\int_{\Omega_{\mathrm{b}}} J \frac{\partial (D^{(1)} - D^{(2)})}{\partial t} \tilde{D}\, d\boldsymbol{X} + \int_{\Omega_{\mathrm{b}}} \beta_{\mathrm{CO}_2} J \mathbf{C}^{-1} \nabla (D^{(1)} - D^{(2)}) \cdot (\nabla \tilde{D})\, d\boldsymbol{X} = \int_{\Omega_{\mathrm{b}}} J \left(f(\theta_{\mathrm{b}})Y - f(\theta_{\mathrm{b}})Y \right) \tilde{D}\, d\boldsymbol{X}. \tag{25}$$

By choosing $\tilde{D} = D^{(1)} - D^{(2)}$ we easily obtain

$$\int_{\Omega_{\mathrm{b}}} J \frac{1}{2} \frac{\partial (D^{(1)} - D^{(2)})^2}{\partial t}\, d\boldsymbol{X} + \int_{\Omega_{\mathrm{b}}} (\beta_{\mathrm{CO}_2} J\, \mathbf{C}^{-1} \nabla (D^{(1)} - D^{(2)})) \cdot (\nabla (D^{(1)} - D^{(2)})\, d\boldsymbol{X} = 0 \tag{26}$$

and, since $J\mathbf{C}^{-1}(\boldsymbol{X})$ is positive definite for any $\boldsymbol{X}$, we get

$$\frac{J_{\min}}{2} \frac{d}{dt} \|D^{(1)} - D^{(2)}\|^2_{L^2(\Omega_{\mathrm{b}})} \leq 0, \tag{27}$$

that, due to the initial conditions, implies $\|D^{(1)} - D^{(2)}\|^2_{L^2(\Omega_{\mathrm{b}})} = 0$ for any $t \in [0, \tau]$. □

4 Discretization scheme

In this section, we first present the time discretization of the problem, that will be at the basis of our numerical scheme. This will also provide a proof of the existence of solutions in a weak sense. Finally, we describe the spatial discretization that we employ in the simulations.

4.1 Time discretization

Let us consider the time interval $[0, \tau]$, we define a time step size Δt and a number of steps n_{steps} such that $\tau = \Delta t\, n_{\mathrm{steps}}$. We use a semi-implicit Euler method to deal with the coupling among the different equations. We denote with the subscript n quantities related to the iteration at the current time. Let us consider (16) that discretized in time reads on each sub-interval

$$\int_{\Omega_{\mathrm{b}}} \rho_{\mathrm{b}} c_{\mathrm{b}}\, J \frac{\theta_{\mathrm{b}_n} - \theta_{\mathrm{b}_{n-1}}}{\Delta t} \tilde{\theta}_{\mathrm{b}_n}\, d\boldsymbol{X} + \int_{\Omega_{\mathrm{b}}} (\beta_{\mathrm{b}}\, J\, \mathbf{C}^{-1} \nabla \theta_{\mathrm{b}_n}) \cdot (\nabla \tilde{\theta}_{\mathrm{b}_n})\, d\boldsymbol{X} = \int_{\Gamma_1} h_{\mathrm{bo}} (\theta_o - \theta_{\mathrm{b}_n}) \tilde{\theta}_{\mathrm{b}_n} |J\, \mathbf{F}^{-\mathsf{T}} \boldsymbol{m}|\, dS + \int_{\Gamma_3} h_{\mathrm{bt}} (\theta_o - \theta_{\mathrm{b}_n}) \tilde{\theta}_{\mathrm{b}_n} |J\, \mathbf{F}^{-\mathsf{T}} \boldsymbol{m}|\, dS \tag{28}$$

where $\theta_{\mathrm{b}_{n-1}}$ is known, as well as $\mathbf{F}$ and J which are computed at the previous time step. Let us now define the bilinear form $a_{\mathrm{b}} : H^1(\Omega_{\mathrm{b}}) \times H^1(\Omega_{\mathrm{b}}) \to \mathbb{R}$ and the linear form $b_{\mathrm{b}} : H^1(\Omega_{\mathrm{b}}) \to \mathbb{R}$ associated with the previous equation:

$$a_{\mathrm{b}}(\theta_{\mathrm{b}_n}, \tilde{\theta}_{\mathrm{b}_n}) = \int_{\Omega_{\mathrm{b}}} \rho_{\mathrm{b}} c_{\mathrm{b}}\, J \frac{\theta_{\mathrm{b}_n}}{\Delta t} \tilde{\theta}_{\mathrm{b}_n}\, d\boldsymbol{X} + \int_{\Omega_{\mathrm{b}}} (\beta_{\mathrm{b}}\, J\, \mathbf{C}^{-1} \nabla \theta_{\mathrm{b}_n}) \cdot (\nabla \tilde{\theta}_{\mathrm{b}_n})\, d\boldsymbol{X} + \int_{\Gamma_1} h_{\mathrm{bo}} \theta_{\mathrm{b}_n} \tilde{\theta}_{\mathrm{b}_n} |J\, \mathbf{F}^{-\mathsf{T}} \boldsymbol{m}|\, dS + \int_{\Gamma_3} h_{\mathrm{bt}} \theta_{\mathrm{b}_n} \tilde{\theta}_{\mathrm{b}_n} |J\, \mathbf{F}^{-\mathsf{T}} \boldsymbol{m}|\, dS, \tag{29}$$

$$b_{\mathrm{b}}(\tilde{\theta}_{\mathrm{b}_n}) = \int_{\Omega_{\mathrm{b}}} \rho_{\mathrm{b}} c_{\mathrm{b}}\, J \frac{\theta_{\mathrm{b}_{n-1}}}{\Delta t} \tilde{\theta}_{\mathrm{b}_n}\, d\boldsymbol{X} + \int_{\Gamma_1} h_{\mathrm{bo}} \theta_o \tilde{\theta}_{\mathrm{b}_n} |J\, \mathbf{F}^{-\mathsf{T}} \boldsymbol{m}|\, dS + \int_{\Gamma_3} h_{\mathrm{bt}} \theta_o \tilde{\theta}_{\mathrm{b}_n} |J\, \mathbf{F}^{-\mathsf{T}} \boldsymbol{m}|\, dS. \tag{30}$$

These forms translate the problem (28) into finding $\theta_{\mathrm{b}_n} \in H^1(\Omega_{\mathrm{b}})$ such that

$$a_{\mathrm{b}}(\theta_{\mathrm{b}_n}, \tilde{\theta}_{\mathrm{b}_n}) = b_{\mathrm{b}}(\tilde{\theta}_{\mathrm{b}_n}) \quad \forall\, \tilde{\theta}_{\mathrm{b}_n} \in H^1(\Omega_{\mathrm{b}}). \tag{31}$$

Concerning the yeast production, by using the discretized solution of the temperature field θ_{b_n}, we can write the discrete version of (9) as

$$Y_n = e^{K_{\mathrm{y}}(\theta_{\mathrm{b}_{n-1}})\Delta t} Y_{n-1}. \tag{32}$$

Finally, the diffusion equation of carbon dioxide (17) becomes

$$\int_{\Omega_{\mathrm{b}}} J\,\frac{D_n - D_{n-1}}{\Delta t}\tilde{D}_n\,d\boldsymbol{X} + \int_{\Omega_{\mathrm{b}}} (\beta_{\mathrm{CO}_2}\,J\,\mathbf{C}^{-1}\nabla D_n)\cdot(\nabla\tilde{D}_n)\,d\boldsymbol{X} + \int_{\Omega_{\mathrm{b}}} J f(\theta_{\mathrm{b}_{n-1}})\,Y_{n-1}\,\tilde{D}_n\,d\boldsymbol{X}, \tag{33}$$

where $\theta_{\mathrm{b}_{n-1}}$ and Y_{n-1} are supposed to be known. The bilinear and linear forms, respectively $a_{\mathrm{D}} : H^1(\Omega_{\mathrm{b}})\times H^1(\Omega_{\mathrm{b}}) \to \mathbb{R}$ and $b_{\mathrm{D}} : H^1(\Omega_{\mathrm{b}}) \to \mathbb{R}$ read

$$a_{\mathrm{D}}(D_n,\tilde{D}_n) = \int_{\Omega_{\mathrm{b}}} J\,\frac{D_n}{\Delta t}\tilde{D}_n\,d\boldsymbol{X} + \int_{\Omega_{\mathrm{b}}} (\beta_{\mathrm{CO}_2}\,J\,\mathbf{C}^{-1}\nabla D_n)\cdot(\nabla\tilde{D}_n)\,d\boldsymbol{X}, \tag{34}$$

$$b_{\mathrm{D}}(\tilde{D}_n) = \int_{\Omega_{\mathrm{b}}} J\,\frac{D_{n-1}}{\Delta t}\tilde{D}_n\,d\boldsymbol{X} + \int_{\Omega_{\mathrm{b}}} J f(\theta_{\mathrm{b}_{n-1}})\,Y_{n-1}\,\tilde{D}_n\,d\boldsymbol{X}. \tag{35}$$

These translate the problem (33) into finding $D_n \in H^1(\Omega_{\mathrm{b}})$ such that

$$a_{\mathrm{D}}(D_n,\tilde{D}_n) = b_{\mathrm{D}}(\tilde{D}_n) \quad \forall\,\tilde{D}_n \in H^1(\Omega_{\mathrm{b}}). \tag{36}$$

Theorem 4.1. *There exists a unique weak solution f_n with components $\theta_{\mathrm{b}_n} \in H^1(\Omega_{\mathrm{b}})$, $Y_n \in L^2(\Omega_{\mathrm{b}})$, and $D_n \in H^1(\Omega_{\mathrm{b}})$ associated with the n-th time step of the problem corresponding to the equations (31),(32),(36).*

Proof. First of all, notice that the yeast production equation (32) is algebraic and its solution exists and is unique for every $\boldsymbol{X}$. Instead, to prove the existence and uniqueness of the solutions of (31) and (36) we only have to check the conditions of continuity and coercivity of the bilinear forms to apply the Lax–Milgram lemma. Notice that the proof of continuity for the linear forms b_{b} and b_D is trivial, thus we skip it. Let us start by verifying the conditions on (29). In what follows c_i with $i \in \mathbb{N}$ denotes a positive constant. The following estimates hold (justified by the considerations in Appendix B):

$$\begin{aligned} |a_{\mathrm{b}}(\theta_{\mathrm{b}_n},\tilde{\theta}_{\mathrm{b}_n})| &\le \int_{\Omega_{\mathrm{b}}} |\rho_{\mathrm{b}} c_{\mathrm{b}} J \frac{\theta_{\mathrm{b}_n}}{\Delta t}\tilde{\theta}_{\mathrm{b}_n}|\,d\boldsymbol{X} + \int_{\Omega_{\mathrm{b}}} |(\beta_{\mathrm{b}} J\mathbf{C}^{-1}\nabla\theta_{\mathrm{b}_n})\cdot\nabla\tilde{\theta}_{\mathrm{b}_n}|\,d\boldsymbol{X} \\ &\quad + \int_{\Gamma_1} |h_{\mathrm{bo}}\theta_{\mathrm{b}_n}\tilde{\theta}_{\mathrm{b}_n}|J\,\mathbf{F}^{-\mathsf{T}}\boldsymbol{m}||\,dS + \int_{\Gamma_3} |h_{\mathrm{bt}}\theta_{\mathrm{b}_n}\tilde{\theta}_{\mathrm{b}_n}|J\,\mathbf{F}^{-\mathsf{T}}\boldsymbol{m}||\,dS \\ &\le c_1|\langle\theta_{\mathrm{b}_n},\tilde{\theta}_{\mathrm{b}_n}\rangle|_{H^1(\Omega_{\mathrm{b}})} + c_2|\langle\theta_{\mathrm{b}_n},\tilde{\theta}_{\mathrm{b}_n}\rangle|_{H^1(\Omega_{\mathrm{b}})} + c_3|\langle\theta_{\mathrm{b}_n},\tilde{\theta}_{\mathrm{b}_n}\rangle|_{H^1(\Omega_{\mathrm{b}})} \\ &\le c_4\|\theta_{\mathrm{b}_n}\|_{H^1(\Omega_{\mathrm{b}})}\,\|\tilde{\theta}_{\mathrm{b}_n}\|_{H^1(\Omega_{\mathrm{b}})} \end{aligned} \tag{37}$$

and

$$\begin{aligned} a_{\mathrm{b}}(\theta_{\mathrm{b}_n},\theta_{\mathrm{b}_n}) &= \int_{\Omega_{\mathrm{b}}} \rho_{\mathrm{b}} c_{\mathrm{b}}\,J\frac{\theta^2_{\mathrm{b}_n}}{\Delta t}\,d\boldsymbol{X} + \int_{\Omega_{\mathrm{b}}} (\beta_{\mathrm{b}} J\mathbf{C}^{-1}\nabla\theta_{\mathrm{b}_n})\cdot\nabla\theta_{\mathrm{b}_n}\,d\boldsymbol{X} \\ &\quad + \int_{\Gamma_1} h_{\mathrm{bo}}\theta^2_{\mathrm{b}_n}|J\,\mathbf{F}^{-\mathsf{T}}\boldsymbol{m}|\,dS + \int_{\Gamma_3} h_{\mathrm{bt}}\theta^2_{\mathrm{b}_n}|J\,\mathbf{F}^{-\mathsf{T}}\boldsymbol{m}|\,dS \\ &\ge c_5\|\theta_{\mathrm{b}_n}\|^2_{L^2(\Omega_{\mathrm{b}})} + c_6\|\nabla\theta_{\mathrm{b}_n}\|^2_{L^2(\Omega_{\mathrm{b}})} \\ &\ge c_7\|\theta_{\mathrm{b}_n}\|^2_{H^1(\Omega_{\mathrm{b}})}. \end{aligned} \tag{38}$$

Let us now consider the diffusion of carbon dioxide (33) and verify the continuity and coercivity of (34) by

$$\begin{aligned} |a_{\mathrm{D}}(D_n,\tilde{D}_n)| &\le \int_{\Omega_{\mathrm{b}}} |J\,\frac{D_n}{\Delta t}\tilde{D}_n|\,d\boldsymbol{X} + \int_{\Omega_{\mathrm{b}}} |(\beta_{\mathrm{CO}_2}\,J\,\mathbf{C}^{-1}\nabla D_n)\cdot(\nabla\tilde{D}_n)|\,d\boldsymbol{X} \\ &\le c_8|\langle D_n,\tilde{D}_n\rangle|_{H^1(\Omega_{\mathrm{b}})} \le c_9\|D_n\|_{H^1(\Omega_{\mathrm{b}})}\,\|\tilde{D}_n\|_{H^1(\Omega_{\mathrm{b}})} \end{aligned} \tag{39}$$

and

$$a_{\mathrm{D}}(D_n, D_n) = \int_{\Omega_{\mathrm{b}}} J\, \frac{D_n^2}{\Delta t}\, d\boldsymbol{X} + \int_{\Omega_{\mathrm{b}}} (\beta_{\mathrm{CO_2}}\, J\, \mathbf{C}^{-1}\nabla D_n) \cdot (\nabla D_n)\, d\boldsymbol{X} \\ \geq c_{10}\|D_n\|^2_{L^2(\Omega_{\mathrm{b}})} + c_{11}\|\nabla D_n\|^2_{L^2(\Omega_{\mathrm{b}})} \geq c_{12}\|D_n\|^2_{H^1(\Omega_{\mathrm{b}})}. \tag{40}$$

With these conditions, we can apply the Lax–Milgram lemma and obtain the existence and uniqueness of solutions for problem (31), (32), (36). □

4.2 Convergence of the time discretization

We can now build a sequence of functions $\{g^{(k)}(\boldsymbol{X},t)\}_k$ which are piece-wise constant and are on each time interval $[t_{n-1}, t_n)$ solutions of the single-time-step equations (31),(32),(36). We set $\Delta t = t_n - t_{n-1} = \tau 2^{-k}$ and define, with

$$g_n^{(k)}(\boldsymbol{X}) = \begin{pmatrix} \theta_{\mathrm{b}_n}^{(k)}(\boldsymbol{X}) \\ Y_n^{(k)}(\boldsymbol{X}) \\ D_n^{(k)}(\boldsymbol{X}) \end{pmatrix}, \tag{41}$$

the global discrete-time solution

$$g^{(k)}(\boldsymbol{X},t) := \sum_{n=0}^{N(k)} g_n^{(k)}(\boldsymbol{X})\chi_{[t_n, t_n+\tau/2^k[}(t), \tag{42}$$

where $n_{\mathrm{steps}} = N(k) = 2^k$ is the number of sub-intervals of $[0,\tau]$. We wish to study the convergence of $\{g^{(k)}(\boldsymbol{X},t)\}_k$ in the Hilbert space $L^2([0,\tau];H)$, where $H := H^1(\Omega_{\mathrm{b}}) \times L^2(\Omega_{\mathrm{b}}) \times H^1(\Omega_{\mathrm{b}})$.

Theorem 4.2. *The sequence $\{g^{(k)}(\boldsymbol{X},t)\}_k$ is bounded and hence admits a weakly convergent sub-sequence in $L^2([0,\tau];H)$.*

Proof. We now compute the appropriate norm for each variable of the discrete problem. In Appendix C we prove the following estimate for $g_n^{(k)}$ when $\Delta t = \tau 2^{-k}$:

$$\Delta t \sum_{n=0}^{N(k)} \|g_n^{(k)}\|_H^2 = \Delta t \sum_{n=0}^{N(k)} \left[\|\theta_{\mathrm{b}_n}^{(k)}\|^2_{H^1(\Omega_{\mathrm{b}})} + \|D_n^{(k)}\|^2_{H^1(\Omega_{\mathrm{b}})} + \|Y_n^{(k)}\|^2_{L^2(\Omega_{\mathrm{b}})}\right] \\ \leq M_{\mathrm{b}_1}\tau\|\theta_{\mathrm{b}0}\|^2_{L^2(\Omega_{\mathrm{b}})} + M_{\mathrm{b}_2}\tau^2\,\|\theta_{\mathrm{o}}\|^2_{L^2(\partial\Omega_{\mathrm{b}})} + M_{\mathrm{b}_3}\|\theta_{\mathrm{b}0}\|^2_{L^2(\Omega_{\mathrm{b}})} + \tau\, M_{\mathrm{b}_4}\|\theta_{\mathrm{o}}\|^2_{L^2(\partial\Omega_{\mathrm{b}})} + M_{D_1}\tau\|D_0\|^2_{L^2(\Omega_{\mathrm{b}})} \\ + M_{D_2}\tau^2\|Y_0\|^2_{L^2(\Omega_{\mathrm{b}})} + M_{D_3}\|D_0\|^2_{L^2(\Omega_{\mathrm{b}})} + M_{D_4}\tau\|Y_0\|^2_{L^2(\Omega_{\mathrm{b}})} + \tau\, c_Y\,\|Y_0\|^2_{L^2(\Omega_{\mathrm{b}})} =: c_1. \tag{43}$$

This estimate is uniform in k and leads to

$$\|g^{(k)}(\boldsymbol{X},t)\|^2_{L^2([0,\tau];H)} = \int_0^\tau \sum_{n=0}^{N(k)} \|g_n^{(k)}(\boldsymbol{X})\|_H^2\ \chi_{[t_n,t_n+\tau/2^k[}(t)\, dt = \sum_{n=0}^{N(k)} \Delta t\|g_n^{(k)}(\boldsymbol{X})\|_H^2 \leq c_1. \tag{44}$$

This proves the boundedness which implies the weak convergence, up to the extraction of a sub-sequence, thanks to the reflexivity of $L^2([0,\tau];H)$. □

Theorem 4.3. *The weak limit $\bar{g}(\boldsymbol{X},t) \in L^2([0,\tau];H)$ provided by the previous theorem is the unique weak solution of (9), (16), (17).*

Proof. Let us write $\bar{g}$ explicitly:

$$\bar{g}(\boldsymbol{X},t) = \begin{pmatrix} \bar{\theta}_{\mathrm{b}}(\boldsymbol{X},t) \\ \bar{Y}(\boldsymbol{X},t) \\ \bar{D}(\boldsymbol{X},t) \end{pmatrix} = \lim_{l\rightharpoonup\infty} \begin{pmatrix} \theta_{\mathrm{b}}^{(k_l)}(\boldsymbol{X},t) \\ Y^{(k_l)}(\boldsymbol{X},t) \\ D^{(k_l)}(\boldsymbol{X},t) \end{pmatrix}. \tag{45}$$

For the sake of simplicity, from now on, we write the index l instead of k_l. Let us consider the heat equation (28), in weak form with $\tilde{g}$ a smooth test function, solved by $\theta_{\mathrm{b}}^{(l)}$ in $L^2([0,\tau];H^1(\Omega_{\mathrm{b}}))$:

$$(46)\qquad \int_0^\tau\int_{\Omega_{\mathrm{b}}}\rho_{\mathrm{b}}c_{\mathrm{b}}\,J\frac{\theta_{\mathrm{b}}^{(l)}(\boldsymbol{X},t)-\theta_{\mathrm{b}}^{(l)}(\boldsymbol{X},t-\Delta t)}{\Delta t}\tilde{g}\,d\boldsymbol{X}\,dt+\int_0^\tau\int_{\Omega_{\mathrm{b}}}(\beta_{\mathrm{b}}\,J\,\mathbf{C}^{-1}\nabla\theta_{\mathrm{b}}^{(l)})\cdot(\nabla\tilde{g})\,d\boldsymbol{X}\,dt$$
$$=\int_0^\tau\int_{\Gamma_1}h_{\mathrm{bo}}(\theta_o-\theta_{\mathrm{b}}^{(l)})\tilde{g}|J\,\mathbf{F}^{-\mathsf{T}}\boldsymbol{m}|\,dS\,dt+\int_0^\tau\int_{\Gamma_3}h_{\mathrm{bt}}(\theta_{\mathrm{o}}-\theta_{\mathrm{b}}^{(l)})\tilde{g}|J\,\mathbf{F}^{-\mathsf{T}}\boldsymbol{m}|\,dS\,dt.$$

Notice that if $\theta_{\mathrm{b}}^{(l)}(\boldsymbol{X},t)$ is weakly convergent in $L^2([0,\tau];H^1(\Omega_{\mathrm{b}}))$ then its gradient is weakly convergent in $L^2([0,\tau];L^2(\Omega_{\mathrm{b}}))$ this, together with the fact that $J\mathbf{C}^{-1}\in L^\infty([0,\tau];L^\infty(\Omega_{\mathrm{b}}))$, allows to pass to the limit in the diffusive term of the equation. The same regularity allows to pass to the limit in the boundary integrals.

In addition, one can easily prove (see Appendix D) that

$$(47)\qquad \int_{\Omega_{\mathrm{b}}}\rho_{\mathrm{b}}c_{\mathrm{b}}\,J\int_0^\tau\frac{\theta_{\mathrm{b}}^{(l)}(\boldsymbol{X},t)-\theta_{\mathrm{b}}^{(l)}(\boldsymbol{X},t-\Delta t)}{\Delta t}\tilde{g}\,dt\,d\boldsymbol{X}$$
$$\underset{l\to\infty}{\longrightarrow}\int_{\Omega_{\mathrm{b}}}\rho_{\mathrm{b}}c_{\mathrm{b}}\,J\Big[\tilde{g}\bar{\theta}_{\mathrm{b}}\Big]_0^\tau\,d\boldsymbol{X}-\int_{\Omega_{\mathrm{b}}}\rho_{\mathrm{b}}c_{\mathrm{b}}\,J\int_0^\tau\frac{\partial\tilde{g}}{\partial t}\bar{\theta}_{\mathrm{b}}\,dt\,d\boldsymbol{X}$$
$$=\int_{\Omega_{\mathrm{b}}}\rho_{\mathrm{b}}c_{\mathrm{b}}\,J\int_0^\tau\frac{\partial\bar{\theta}_{\mathrm{b}}}{\partial t}\tilde{g}\,dt\,d\boldsymbol{X}.$$

This proves that $\bar{\theta}_{\mathrm{b}}$ is a weak solution of (16). Completely analogous considerations prove that $\bar{D}$ is a weak solution of (17). In the limit $\Delta t\to 0$, equation (32) is equivalent to $Y_n-Y_{n-1}=\Delta tK_{\mathrm{y}}(\theta_{\mathrm{b}_{n-1}})Y_{n-1}$. With this observation and considering the uniform boundedness of K_{y}, applying again the arguments above, we get that $\bar{Y}$ is a solution of the weak form of equation (9). The combining of these results with Theorem 3.1 is the existence and uniqueness of the continuous problem stated by (9), (16), (17). □

4.3 Spatial discretization

For the spatial discretization we use the finite-element method (see [20] for some references) on an unstructured mesh, made of tetrahedra with average diameter h. We define the spaces V_h, in which we approximate the vectorial deformation $\boldsymbol{u}$ with Lagrangian elements P1, and W_h, where the temperature of the dough θ_{b}, the yeasts concentration Y and the CO_2 concentration D are approximated with P1 elements as well. Notice that working with material coordinates allows us to have a fixed domain independent of the volume deformation.

5 Numerical results

The simulations are performed in Python using the library FEniCSx and the results are analyzed with the software ParaView. The coupled discretized equations are integrated with a semi-implicit Euler method. At each time step, we minimize the elastic energy with respect to the deformation map $\boldsymbol{u}$. From such computation we update the value of J and $\mathbf{C}$. Then we solve the equations for θ_{b}, Y, and D, and consequently update J_{ref} and the elastic moduli E, λ, and μ (see Table 2).

The material domain Ω_{b} is a box with sides of centimeters $40\times 16\times 16$. This is the actual shape of a type of baking trays used in industrial production. Since the leavening process of the baking paste takes place within those trays, it is convenient to use the same shape for the material domain. An unstructured mesh of the domain with average element diameter $h=0.1\,\mathrm{cm}$ was chosen after checking the mesh convergence of the solution to a test heat equation. A time step of 1 s, well within the bounds of the standard CFL condition for the heat equation, was used, since the CO_2 diffusion equation poses less restrictive bounds. Given that we are interested in simulating leavening times of the order of two hours and the computational times for each iteration is of the order of a few seconds, the total time of each simulation is quite reasonable. In Figures 2 and 3 we show examples of the evolution of the deformation map and the temperature field of our simulations when the initial yeast concentration is set to 0.4 and the leavening chamber temperature is set to 25°C.

Table 2. Semi-implicit iterative scheme used to solve the discretized model.

Algorithm:
for $n = 0, \ldots, n_{\text{steps}}$: → **solve** the **elasticity** eq. (iterative nonlinear solver) → **update** value of J and $\mathbf{C}$ → **solve** the heat eq. in the baking paste → **compute** the yeasts growth rate → **solve** the diffusion eq. for the CO_2 concentration → **compute** the volume occupied by CO_2 → **update** the value of J_{ref} and the elastic stiffness end loop

Table 3. Fixed input parameters used in the simulations.

Value	**Units**	**Description**
$E_0 = 10$	Pa	Young's modulus
$\nu = 0.48$		Possion's ratio
$\boldsymbol{B} = (0, 0, -9.8)$	$\mathrm{m\,s^{-2}}$	body force, gravity
$\theta_0 = 18$	$^\circ\mathrm{C}$	initial temperature of the baking paste
$\beta_{\text{b}} = 0.4125$	$\mathrm{J\,K^{-1}\,m^{-1}\,s^{-1}}$	thermal conductivity, weighted average between the water and flour value respectively
$h_{\text{bo}} = 50$	$\mathrm{J\,K^{-1}\,m^{-2}\,s^{-1}}$	bread-to-air heat transfer coefficient
$h_{\text{bt}} = 60$	$\mathrm{J\,K^{-1}\,m^{-2}\,s^{-1}}$	bread-to-baking tray heat transfer coefficient
$c_{\text{b}} = 4186$	$\mathrm{J\,K^{-1}\,kg^{-1}}$	specific heat water
$\rho_{\text{b}} = 170$	$\mathrm{kg\,m^{-3}}$	bread density empirical measure
$\beta_{CO_2} = 1.e-4$	$\mathrm{m^2\,s^{-1}}$	diffusivity of concentration of CO_2
$\lambda_{\text{y}} = 0.00005$	$\mathrm{s^{-1}}$	calibrated following Ref. [10]
$\lambda_{CO_2} = 2.e-6$	$\mathrm{s^{-1}}$	
$R = 8.31$	$\mathrm{J\,mol^{-1}\,K^{-1}}$	
$n_{\text{mol}} = 1/44$		number of moles contained in a gram of CO_2
$V_0^{1g} = 4{,}38e-6$	$\mathrm{m^3}$	total volume of a gram of bread paste $= W_{\text{rate}}\,V_{\text{w}} + F_{\text{rate}}\,V_{\text{f}} = (1 - F_{\text{rate}})\,V_{\text{w}} + F_{\text{rate}}\,V_{\text{f}}$
$P_{\text{diss}} = 30$	$\mathrm{W^\circ C^{-1}}$	dissipated power per $^\circ$C from manufacturer data sheet

We perform simulations to compare the leavening process in the following different conditions:

- the temperature of the leavening chamber set to 18°C, 25°C, 30°C, or 45°C;
- the yeast initial concentration set to 2%, 3%, or 4%.

The other input parameters that are fixed throughout our tests are listed in Table 3. Regarding the value of the specific heat of the baking paste, we chose it equal to the one of water because the paste remains wet during leavening and the presence of flour does not affect in a relevant way this coefficient. We would need to change it significantly if we were to describe the cooking process, in which the paste dries out. In our model we assume that yeast produces CO_2 within a temperature range between 5°C and 45°C with a peak of production at 25°C (see Figure 1(b)).

From the results of the simulation we can interrogate the model to understand how much time is needed to achieve a given increase in volume under different settings (see Figure 4). While the effect of yeast concentration is quite obvious (faster growth with more yeast), the temperature of the leavening chamber affects the volume expansion in a less trivial way. Indeed, setting the temperature too far beyond the peak of CO_2 production results in a rather fast expansion for short times followed by a substantial loss of the leavening capability, with a consequent saturation of the growth, as shown in Figure 4(d). This would bear little consequences if the target increase were 50%, but would be a crucial piece of information if one needed to reach a 200% expansion (see the horizontal dotted lines in Figure 4), that

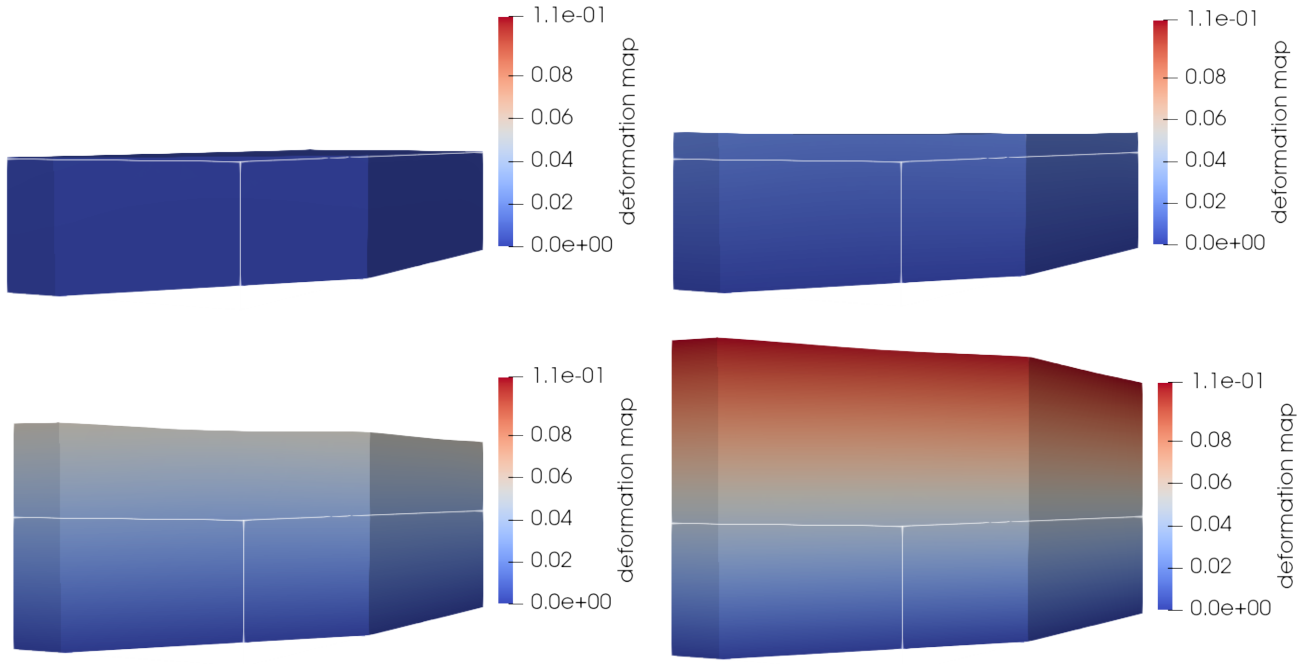

Figure 2. In these plots we see the evolution of the growing elastic paste, which is obtained by solving the elasticity equation of our simulations when the initial yeast concentration is set to 0.4 and the leavening chamber temperature is set to 25°C. In particular, snapshots are taken at $t = 100\,\mathrm{s}$, $t = 400\,\mathrm{s}$, $t = 1200\,\mathrm{s}$ and $t = 2500\,\mathrm{s}$.

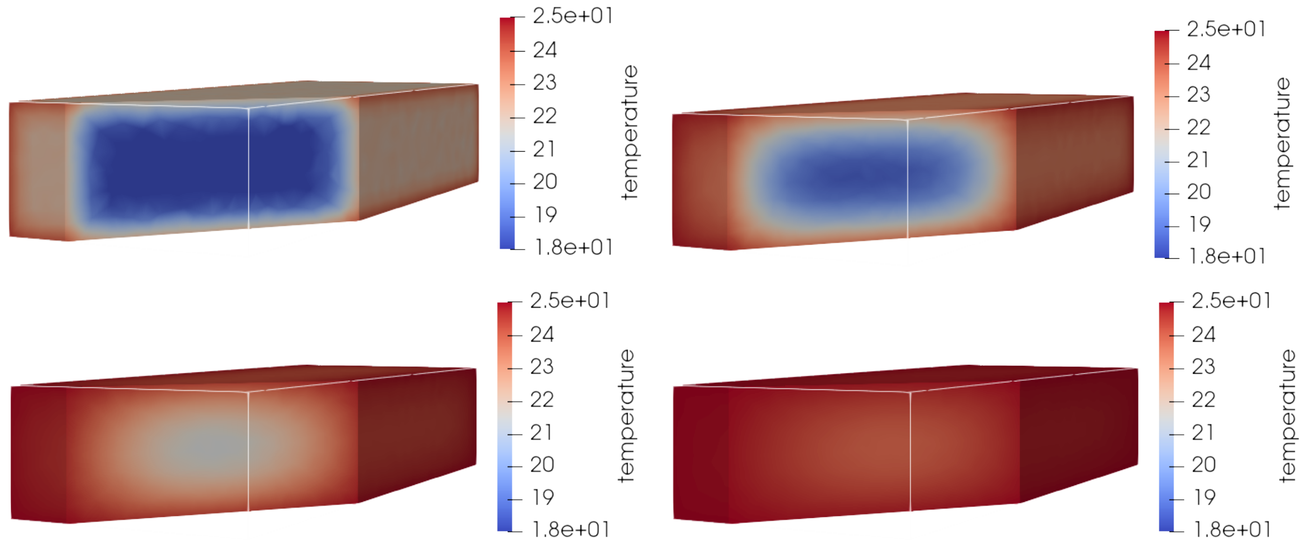

Figure 3. In these plots we see the evolution of the temperature field over the reference domain, obtained by solving the heat equation in our simulations when the initial yeast concentration is set to 0.4 and the leavening chamber temperature is set to 25°C. The temperature field refers to times $t = 100\,\mathrm{s}$, $t = 400\,\mathrm{s}$, $t = 1200\,\mathrm{s}$ and $t = 2500\,\mathrm{s}$.

would be impossible with a temperature of 45°C. The most rapid growth is achieved with 30°C, a little above the peak CO_2 production temperature, see Figure 4(c).

The final goal of this study is to provide a tool for the prediction of energy consumption in industrial processes. We then consider that the energy used by the leavening process is the sum of the energy absorbed by the baking paste

$$\mathcal{E}_{\mathrm{b}}(t) = \int_{\Omega_{\mathrm{b}}} \rho_{\mathrm{b}} c_{\mathrm{b}} \theta_{\mathrm{b}}(\boldsymbol{X}, t)\, d\boldsymbol{X} - \mathcal{E}_0, \tag{48}$$

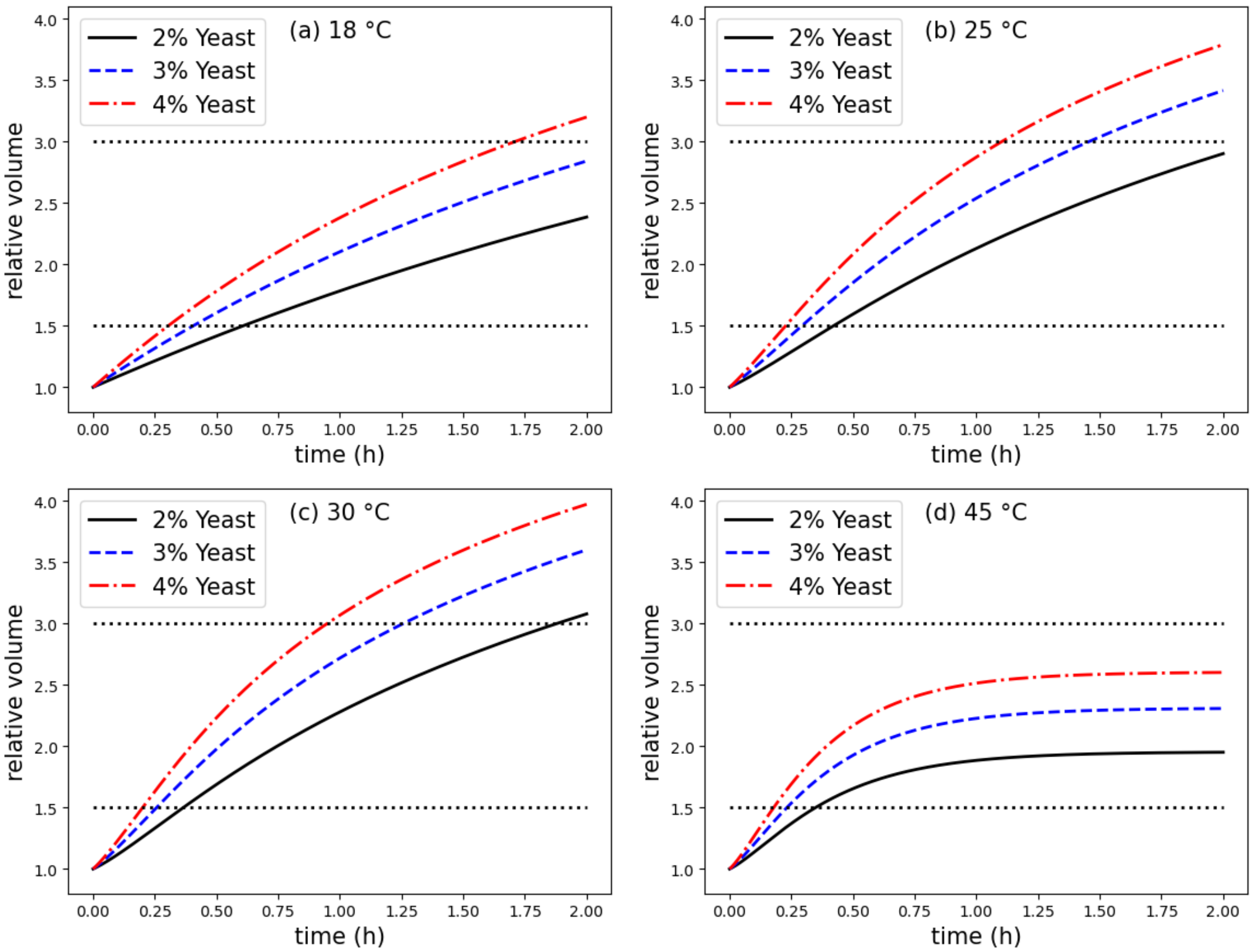

Figure 4. Yeast concentration and the temperature of the leavening chamber influence the volumetric expansion in different ways. By considering the relative volume expansion $v(t)/v_0$ as a function of time for different yeast concentrations and temperatures, as indicated on the graphs, we can predict the time necessary to reach a given expansion, if at all possible. Horizontal dotted lines represent two possible target volumes: $v_f = 1.5v_0$ or $v_f = 3v_0$.

where $\mathcal{E}_0 = \int_{\Omega_b} \rho_b c_b \theta_0(\boldsymbol{X})\, d\boldsymbol{X}$ is the initial thermal energy, and the energy $\mathcal{E}_{\text{diss}}$ dissipated by the leavening chamber simply to reach and keep the temperature θ_o starting from θ_0 and for a time t, that is given by

$$\mathcal{E}_{\text{diss}}(t) = P_{\text{diss}}\, t\, (\theta_o - \theta_0), \tag{49}$$

where the coefficient P_{diss} is the dissipated power per °C, a value that is commonly found in the data sheet of industrial leavening machines.

We then compute the energy expenditure as a function of time for all the performed experiments (Figure 5). First of all, we observe that the yeast concentration does not affect in a measurable way the energy required during the process, but does impact on the time necessary to reach any given target volume. By marking on the energy consumption curves the point at which an expansion of either 50% or 200% is reached (Figure 5, panel (a) or (b), respectively), we see that there is a competition between the energetic cost and the time to target for any fixed yeast concentration. The resulting energy consumption to reach two different target volumes for all the experiments is summarized in Table 5. It is worth noticing that the consumed energy at 18°C is *zero* since it corresponds to the room temperature in the laboratory and the leavening machine does not need to spend additional energy. Practical considerations based on this kind of simulation can lead to more effective strategies for the optimization of the energy consumption given the time constraint due to production needs.

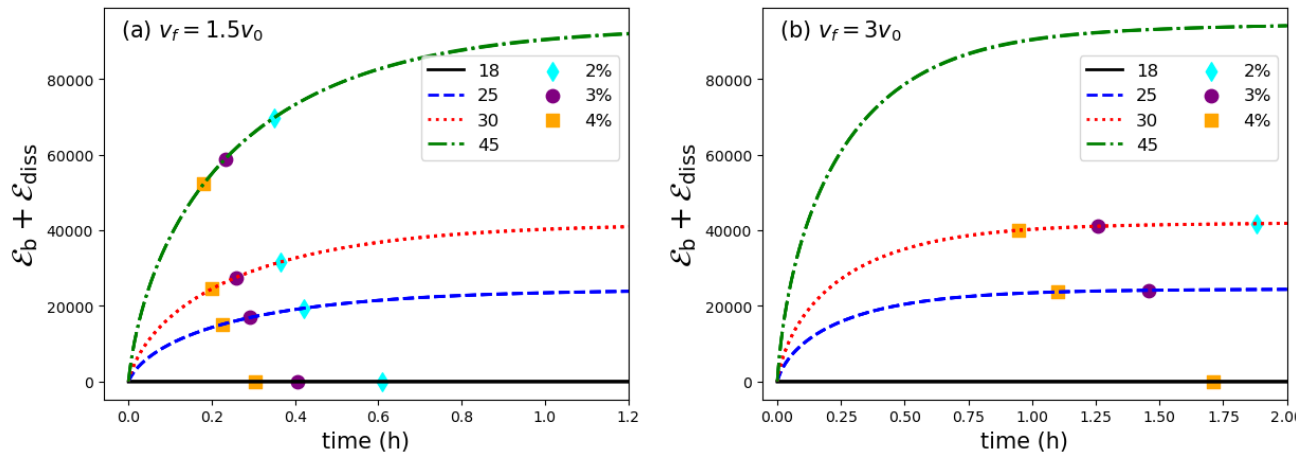

Figure 5. The time to reach a target volume increases upon decreasing the temperature and energy consumption, while the yeast concentration affects only the time to target. The energy consumption is plotted as a function of time for different system settings (see legend). The symbols on each curve represent the reaching of the target volume. In (a) we consider a target expansion of 50% (with $v_f = 1.5v_0$), while in (b) a 200% expansion (with $v_f = 3v_0$).

Table 4. Energy consumption to reach the target volume v_f for all the experiments.

$\mathcal{E}_b + \mathcal{E}_{diss}$ $v_f = 1.5\,v_0$	Temperature			
Yeast	18°C	25°C	30°C	45°C
0.2%	0 J	19405 J	31671 J	69790 J
0.3%	0 J	16932 J	27492 J	58803 J
0.4%	0 J	15157 J	24522 J	52215 J

$\mathcal{E}_b + \mathcal{E}_{diss}$ $v_f = 3\,v_0$	Temperature			
Yeast	18°C	25°C	30°C	45°C
0.2%	-	-	41733 J	-
0.3%	-	24135 J	41066 J	-
0.4%	0 J	23731 J	40085 J	-

We propose our approach as a method that can be applied to realistic situations when measurements of the relevant parameters are available. Indeed, suitable calibrations of all the elements of our model can lead to different quantitative predictions.

In Ref. [21], the authors study the different behaviors of leavening for different values of the temperature of the chamber and of the water percentage. At this stage, the water content appears in our model only in the calculation of the volume of a gram of dough, so it is difficult to make a full comparison with the results of that study. However, we can get close results when we set the leavening temperature to $\theta_o = 30$ °C, the yeast concentration to $Y_0 = 5\%$, and by calibrating the value of the initial specific volume of bread at $V_0^{1g} = 3e-6$ m^3. The inclusion of the moisture equation is a possible future development that would allow to reproduce more closely certain data. We can find a better agreement with the data provided in Ref. [22], where the authors calibrate their model parameters to have a correspondence with experimental values. In our case, to achieve results close to theirs, we can set $\theta_0 = 26.5$ °C, $\theta_o = 28$ °C, $Y_0 = 2\%$ and the initial specific volume of bread at $V_0^{1g} = 2.5e-6$ m^3.

6 Conclusions

We presented a work aimed at modelling the industrial process of bread leavening with the goal of predicting energy consumption. We developed a mathematical model that takes into account the deformation of the dough, heat transfer, the metabolism of yeast, and carbon dioxide production and diffusion by describing leavening from a macroscopic point of view. This implies treating CO_2 in the perspective of representing the volumetric expansion and neglecting vibrations of the baking paste.

The coupling among equations is managed by working in material coordinates, and by updating the elastic stiffness to the current value of carbon dioxide to describe structural changes in dough mechanics. Our numerical simulations were performed to show how the model can be used to identify the energy consumption necessary to achieve a target volume expansion. With this information it is possible to plan the production strategy to optimize energy consumption within practical constraints.

A first improvement of this work could be to replicate the entire bread baking process. In such a case, we have to develop a model of cooking, where, differently form what happens in leavening, the effects of higher temperatures on the mechanics and the chemistry of the dough (such as humidity loss, denaturation, and hardening), requires adding a moisture equation, as well as other terms to describe the energy and the water mass lost by the baking paste through evaporation and boiling phenomena.

A further evolution of this work would be to use of our model for the development of digital twins for leavening chambers to achieve an automated energy optimization. Indeed, we plan to use this model to address the formulation of an inverse problem to be solved in systems embedded in the chamber hardware by exploiting physics-aware soft-sensors, similarly to what has been done for other applications [23]. Moreover, we plan to build a surrogate model that will be computationally cheaper than our numerical model, and that would allow to run simulations in real time during the leavening process, which is a main goal of digital twins [14].

Acknowledgements

The authors would like to thank Fabio Marcuzzi for many useful discussions on the topics of this research. L.R. acknowledges the financial support of the Italian Government through the "Programma Operativo Nazionale Ricerca e Innovazione" 2014-2020 (CCI 2014IT16M2OP005), fellowship number DOT1319984-2. The work of L.R. is partially supported by the "Gruppo Nazionale per il Calcolo Scientifico" (GNCS - INdAM). The work of G.G.G. is partially supported by the "Gruppo Nazionale per la Fisica Matematica" (GNFM - INdAM).

A Equations in material coordinates

Let us denote with $\boldsymbol{X}$ the material coordinates on Ω_{b} and with $\boldsymbol{x}$ the spatial one. In the following we write in material coordinates a general field $\theta : \Omega_{\mathrm{b}} \times \mathbb{R} \to \mathbb{R}$ with its spatial counterpart $\hat{\theta}$ linked by the following relations:

$$\theta(\boldsymbol{X}, t) = \hat{\theta}(\boldsymbol{u}(\boldsymbol{X}, t), t), \qquad \hat{\theta}(\boldsymbol{x}, t) = \theta(\boldsymbol{u}^{-1}(\boldsymbol{x}, t), t), \tag{50}$$

where we denote with $\boldsymbol{u}$ the function that assigns at each time, to each material point $\boldsymbol{X}$ a new point $\boldsymbol{x}$ as the spatial point occupied by $\boldsymbol{X}$ at time t. Concerning the gradients, we have

$$\nabla_{\boldsymbol{X}} \boldsymbol{u} = \mathsf{F}, \qquad \nabla_{\boldsymbol{x}} = \mathsf{F}^{-\mathsf{T}} \nabla_{\boldsymbol{X}}, \tag{51}$$

$$\nabla_{\boldsymbol{x}} \hat{\theta} = \nabla_{\boldsymbol{X}} \theta \Big(\frac{\partial \boldsymbol{u}(\boldsymbol{x}, t)}{\partial \boldsymbol{X}} \Big)^{-1} = \mathsf{F}^{-\mathsf{T}} \nabla_{\boldsymbol{X}} \theta, \tag{52}$$

and for the time derivatives we obtain

$$\begin{aligned} \frac{\partial \hat{\theta}}{\partial t}(\boldsymbol{x}, t) &= \frac{\partial \theta(\boldsymbol{u}^{-1}(\boldsymbol{x}, t), t)}{\partial t} = \frac{\partial \theta(\boldsymbol{u}^{-1}(\boldsymbol{x}, t), t)}{\partial \boldsymbol{X}} \frac{\partial \boldsymbol{u}^{-1}(\boldsymbol{x}, t)}{\partial t} + \frac{\partial \theta(\boldsymbol{u}^{-1}(\boldsymbol{x}, t), t)}{\partial t} \\ &= \nabla_{\boldsymbol{X}} \theta \frac{\partial \boldsymbol{u}^{-1}(\boldsymbol{x}, t)}{\partial t} + \frac{\partial \theta(\boldsymbol{u}^{-1}(\boldsymbol{x}, t), t)}{\partial t} = \nabla_{\boldsymbol{X}} \theta \frac{\partial \boldsymbol{u}^{-1}(\boldsymbol{x}, t)}{\partial t} + \frac{\partial \theta(\boldsymbol{X}, t)}{\partial t} = \frac{\partial \theta(\boldsymbol{X}, t)}{\partial t} \end{aligned} \tag{53}$$

where the last equality holds because we consider a static deformation of the bread, hence the absence of convective terms. Finally, the term corresponding to the divergence on the heat flux satisfies

$$\operatorname{div}_{\boldsymbol{x}}(\nabla_{\boldsymbol{x}} \hat{\theta}) = \operatorname{div}_{\boldsymbol{x}}(\mathsf{F}^{-\mathsf{T}} \nabla_{\boldsymbol{X}} \theta) = \operatorname{div}_{\boldsymbol{X}}(\mathsf{F}^{-1} \mathsf{F}^{-\mathsf{T}} J \nabla_{\boldsymbol{X}} \theta) = \operatorname{div}_{\boldsymbol{X}}(\mathsf{C}^{-1} J \nabla_{\boldsymbol{X}} \theta). \tag{54}$$

The volume of the spatial domain $\boldsymbol{u}(\Omega_\mathrm{b})$ and surface $\partial\boldsymbol{u}(\Omega_\mathrm{b})$ in material coordinates can be computed as

$$\int_{\boldsymbol{u}(\Omega_\mathrm{b})} d\boldsymbol{x} = \int_{\Omega_\mathrm{b}} J\, d\boldsymbol{X}, \tag{55}$$

$$\int_{\partial\boldsymbol{u}(\Omega_\mathrm{b})} ds = \int_{\partial\Omega_\mathrm{b}} |J\mathsf{F}^{-\mathsf{T}}\boldsymbol{m}|\, dS, \tag{56}$$

where $\boldsymbol{m}$ is the unit outer normal $\partial\Omega_\mathrm{b}$. With the foregoing identities we can easily obtain equation (5) of the main text.

B Details about estimates

Given that the deformation is fixed over the time interval $[0,\tau]$, we can assume the boundedness condition $J\mathsf{C}^{-1} \in L^\infty([0,\tau]; L^\infty(\Omega_\mathrm{b}))$. We also assume $\mathsf{A} := J\,\mathsf{C}^{-1}$ symmetric and positive-definite, so that there exists the smallest eigenvalue $c_A(\boldsymbol{X}) > 0$ and the largest one $C_A(\boldsymbol{X}) > 0$. We then obtain the following estimates for the generic functions θ and $\tilde\theta$

$$\begin{aligned}\int_{\Omega_\mathrm{b}} (\beta\, J\,\mathsf{C}^{-1}\nabla\theta)\cdot\nabla\tilde\theta\, d\boldsymbol{X} &= \int_{\Omega_\mathrm{b}} \beta\nabla\tilde\theta\cdot\mathsf{A}(\nabla\theta)\, d\boldsymbol{X} \ge \int_{\Omega_\mathrm{b}} c_A(\boldsymbol{X})\beta\nabla\tilde\theta\cdot(\nabla\theta)\, d\boldsymbol{X} \\ &= \int_{\Omega_\mathrm{b}} \beta\, c_A(\boldsymbol{X})(\nabla\theta\cdot\nabla\tilde\theta)\, d\boldsymbol{X} \ge \beta \min_{\boldsymbol{X}\in\Omega_\mathrm{b}} c_A(\boldsymbol{X})\langle\nabla\theta,\nabla\tilde\theta\rangle_{L^2(\Omega_\mathrm{b})} \\ &\ge c\langle\nabla\theta,\nabla\tilde\theta\rangle_{L^2(\Omega_\mathrm{b})},\end{aligned} \tag{57}$$

$$\begin{aligned}\int_{\Omega_\mathrm{b}} (\beta\, J\,\mathsf{C}^{-1}\nabla\theta)\cdot\nabla\tilde\theta\, d\boldsymbol{X} &\le \int_{\Omega_\mathrm{b}} \beta\nabla\tilde\theta\cdot\mathsf{A}(\nabla\theta)\, d\boldsymbol{X} \le \int_{\Omega_\mathrm{b}} C_A(\boldsymbol{X})\beta\nabla\tilde\theta\cdot(\nabla\theta)\, d\boldsymbol{X} \\ &\le \int_{\Omega_\mathrm{b}} \beta\, C_A(\boldsymbol{X})(\nabla\theta\cdot\nabla\tilde\theta)\, d\boldsymbol{X} \le \beta \max_{\boldsymbol{X}\in\Omega_\mathrm{b}} C_A(\boldsymbol{X})\langle\nabla\theta,\nabla\tilde\theta\rangle_{L^2(\Omega_\mathrm{b})} \\ &\le C\langle\nabla\theta,\nabla\tilde\theta\rangle_{L^2(\Omega_\mathrm{b})}.\end{aligned} \tag{58}$$

In a similar way, we get the estimates

$$\int_{\Omega_\mathrm{b}} J\,\theta\,\tilde\theta\, d\boldsymbol{X} \ge \min_{\boldsymbol{X}\in\Omega_\mathrm{b}} J\langle\theta,\tilde\theta\rangle_{L^2(\Omega_\mathrm{b})} \ge J_{\min}\langle\theta,\tilde\theta\rangle_{L^2(\Omega_\mathrm{b})} \ge 0, \tag{59}$$

$$\int_{\Omega_\mathrm{b}} J\,\theta\,\tilde\theta\, d\boldsymbol{X} \le \max_{\boldsymbol{X}\in\Omega_\mathrm{b}} J\langle\theta,\tilde\theta\rangle_{L^2(\Omega_\mathrm{b})} \le J_{\max}\langle\theta,\tilde\theta\rangle_{L^2(\Omega_\mathrm{b})}, \tag{60}$$

and, given that the boundedness of $J\mathsf{C}^{-1}$ implies the boundedness of $J\mathsf{F}^{-\mathsf{T}}$, we also have

$$\int_{\partial\Omega_\mathrm{b}} |J\mathsf{F}^{-\mathsf{T}}\boldsymbol{m}|\tilde\theta\, dS \ge C\int_{\partial\Omega_\mathrm{b}} \tilde\theta\, dS, \tag{61}$$

$$\int_{\partial\Omega_\mathrm{b}} |J\mathsf{F}^{-\mathsf{T}}\boldsymbol{m}|\tilde\theta\, dS \le c\int_{\partial\Omega_\mathrm{b}} \tilde\theta\, dS. \tag{62}$$

C Estimates for the time discretization

C.1 Heat equation in the bread

We first consider estimates useful for equation (28). We have

$$\frac{\rho_{\mathrm{b}}c_{\mathrm{b}}}{2\Delta t}\|\sqrt{J}\theta_{\mathrm{b}_n}\|^2_{L^2(\Omega_{\mathrm{b}})}+\tilde\beta\|\sqrt{J}\nabla\theta_{\mathrm{b}_n}\|^2_{L^2(\Omega_{\mathrm{b}})}+\bar h\|J\theta_{\mathrm{b}_n}\|^2_{L^2(\partial\Omega_{\mathrm{b}})}\le\frac{\rho_{\mathrm{b}}c_{\mathrm{b}}}{2\Delta t}\|\sqrt{J}\theta_{\mathrm{b}_{n-1}}\|^2_{L^2(\Omega_{\mathrm{b}})}+\tilde h\|J\theta_{\mathrm{o}}\theta_{\mathrm{b}_n}\|_{L^1(\partial\Omega_{\mathrm{b}})},$$

$$\frac{\rho_{\mathrm{b}}c_{\mathrm{b}}}{2\Delta t}\|\sqrt{J}\theta_{\mathrm{b}_n}\|^2_{L^2(\Omega_{\mathrm{b}})}+\tilde\beta\|\sqrt{J}\nabla\theta_{\mathrm{b}_n}\|^2_{L^2(\Omega_{\mathrm{b}})}+\bar h\|J\theta_{\mathrm{b}_n}\|^2_{L^2(\partial\Omega_{\mathrm{b}})}\le\frac{\rho_{\mathrm{b}}c_{\mathrm{b}}}{2\Delta t}\|\sqrt{J}\theta_{\mathrm{b}_{n-1}}\|^2_{L^2(\Omega_{\mathrm{b}})}+\tilde h\|\theta_{\mathrm{o}}\|_{L^2(\partial\Omega_{\mathrm{b}})}\|J\theta_{\mathrm{b}_n}\|_{L^2(\partial\Omega_{\mathrm{b}})},\tag{63}$$

$$\frac{\rho_{\mathrm{b}}c_{\mathrm{b}}}{2\Delta t}\|\sqrt{J}\theta_{\mathrm{b}_n}\|^2_{L^2(\Omega_{\mathrm{b}})}+\tilde\beta\|\sqrt{J}\nabla\theta_{\mathrm{b}_n}\|^2_{L^2(\Omega_{\mathrm{b}})}+\bar h\|J\theta_{\mathrm{b}_n}\|^2_{L^2(\partial\Omega_{\mathrm{b}})}\le\frac{\rho_{\mathrm{b}}c_{\mathrm{b}}}{2\Delta t}\|\sqrt{J}\theta_{\mathrm{b}_{n-1}}\|^2_{L^2(\Omega_{\mathrm{b}})}+\tilde h\Big(\frac{1}{2\varepsilon}\|\theta_{\mathrm{o}}\|^2_{L^2(\partial\Omega_{\mathrm{b}})}+\frac{\varepsilon}{2}\|J\theta_{\mathrm{b}_n}\|^2_{L^2(\partial\Omega_{\mathrm{b}})}\Big).\tag{64}$$

If we chose $\varepsilon=\frac{2\bar h}{\tilde h}$ we get

$$\frac{\rho_{\mathrm{b}}c_{\mathrm{b}}}{2\Delta t}\|\sqrt{J}\theta_{\mathrm{b}_n}\|^2_{L^2(\Omega_{\mathrm{b}})}+\tilde\beta\|\sqrt{J}\nabla\theta_{\mathrm{b}_n}\|^2_{L^2(\Omega_{\mathrm{b}})}\le\frac{\rho_{\mathrm{b}}c_{\mathrm{b}}}{2\Delta t}\|\sqrt{J}\theta_{\mathrm{b}_{n-1}}\|^2_{L^2(\Omega_{\mathrm{b}})}+\tilde h\frac{1}{2\varepsilon}\|\theta_{\mathrm{o}}\|^2_{L^2(\partial\Omega_{\mathrm{b}})},\tag{65}$$

$$\frac{\rho_{\mathrm{b}}c_{\mathrm{b}}}{2\Delta t}\|\sqrt{J}\theta_{\mathrm{b}_n}\|^2_{L^2(\Omega_{\mathrm{b}})}\le\frac{\rho_{\mathrm{b}}c_{\mathrm{b}}}{2\Delta t}\|\sqrt{J}\theta_{\mathrm{b}_{n-1}}\|^2_{L^2(\Omega_{\mathrm{b}})}+\frac{\tilde h}{2\varepsilon}\|\theta_{\mathrm{o}}\|^2_{L^2(\partial\Omega_{\mathrm{b}})}.\tag{66}$$

Thus, by summing over s we obtain:

$$\Delta t\sum_{s=1}^{n}\|\theta^{(k)}_{\mathrm{b}_s}\|^2_{L^2(\Omega_{\mathrm{b}})}\le M_{\mathrm{b}_1}\tau\|\theta_{\mathrm{b}0}\|^2_{L^2(\Omega_{\mathrm{b}})}+M_{\mathrm{b}_2}\tau^2\,\|\theta_{\mathrm{o}}\|^2_{L^2(\partial\Omega_{\mathrm{b}})}.\tag{67}$$

where $\tau=N(k)\,\Delta t$.

Moreover, by summing (65) over s we also obtain:

$$\frac{\rho_{\mathrm{b}}c_{\mathrm{b}}}{2\Delta t}\|\sqrt{J}\theta_{\mathrm{b}_n}\|^2_{L^2(\Omega_{\mathrm{b}})}+\sum_{s=1}^{n}\tilde\beta\|\sqrt{J}\nabla\theta_{\mathrm{b}_s}\|^2_{L^2(\Omega_{\mathrm{b}})}\le\frac{\rho_{\mathrm{b}}c_{\mathrm{b}}}{2\Delta t}\|\sqrt{J}\theta_{\mathrm{b}0}\|^2_{L^2(\Omega_{\mathrm{b}})}+n\,\tilde h\frac{1}{2\varepsilon}\|\theta_{\mathrm{o}}\|^2_{L^2(\partial\Omega_{\mathrm{b}})},\tag{68}$$

$$\sum_{s=1}^{n}\tilde\beta\|\sqrt{J}\nabla\theta_{\mathrm{b}_s}\|^2_{L^2(\Omega_{\mathrm{b}})}\le\frac{\rho_{\mathrm{b}}c_{\mathrm{b}}}{2\Delta t}\|\sqrt{J}\theta_{\mathrm{b}0}\|^2_{L^2(\Omega_{\mathrm{b}})}+n\,\tilde h\frac{1}{2\varepsilon}\|\theta_{\mathrm{o}}\|^2_{L^2(\partial\Omega_{\mathrm{b}})},\tag{69}$$

$$\Delta t\sum_{s=1}^{n}\tilde\beta\|\sqrt{J}\nabla\theta_{\mathrm{b}_s}\|^2_{L^2(\Omega_{\mathrm{b}})}\le\frac{\rho_{\mathrm{b}}c_{\mathrm{b}}}{2}\|\sqrt{J}\theta_{\mathrm{b}0}\|^2_{L^2(\Omega_{\mathrm{b}})}+\tau\,\tilde h\frac{1}{2\varepsilon}\|\theta_{\mathrm{o}}\|^2_{L^2(\partial\Omega_{\mathrm{b}})},\tag{70}$$

$$\Delta t\sum_{s=1}^{n}\|\nabla\theta_{\mathrm{b}_s}\|^2_{L^2(\Omega_{\mathrm{b}})}\le M_{b_3}\|\theta_{\mathrm{b}0}\|^2_{L^2(\Omega_{\mathrm{b}})}+\tau\,M_{b_4}\|\theta_{\mathrm{o}}\|^2_{L^2(\partial\Omega_{\mathrm{b}})}.\tag{71}$$

C.2 Production of yeast

We then consider estimates useful for equation (32). Starting from

$$\begin{aligned}\|Y_n\|^2_{L^2(\Omega_{\mathrm{b}})}&=\|e^{K_{\mathrm{y}}(\theta_{\mathrm{b}_{n-1}})\Delta t}\;Y_{n-1}\|^2_{L^2(\Omega_{\mathrm{b}})}\\&\le\|e^{\max K_{\mathrm{y}}\Delta t}Y_{n-1}\|^2_{L^2(\Omega_{\mathrm{b}})}\\&=|e^{\max K_{\mathrm{y}}\Delta t}|^2\|Y_{n-1}\|^2_{L^2(\Omega_{\mathrm{b}})}\\&\le|e^{\max K_{\mathrm{y}}\Delta t}|^{2n}\|Y_0\|^2_{L^2(\Omega_{\mathrm{b}})}\\&\le|e^{c\tau}|\,\|Y_0\|^2_{L^2(\Omega_{\mathrm{b}})},\end{aligned}\tag{72}$$

by computing the sum over s we obtain

$$\Delta t\sum_{s=1}^{n}\|Y^{(k)}_s\|^2_{L^2(\Omega_{\mathrm{b}})}\le\Delta t\sum_{s=1}^{n}|e^{c\tau}|\,\|Y_0\|^2_{L^2(\Omega_{\mathrm{b}})}\le\tau\,c_Y\,\|Y_0\|^2_{L^2(\Omega_{\mathrm{b}})}.\tag{73}$$

C.3 Diffusion and production of carbon dioxide

We finally consider estimates useful for equation (33), which are

$$\frac{1}{\Delta t}\|\sqrt{J}D_n\|^2_{L^2(\Omega_\mathrm{b})} + \tilde{\beta}\|\sqrt{J}\nabla D_n\|^2_{L^2(\Omega_\mathrm{b})} \le \frac{1}{2\Delta t}\|\sqrt{J}D_n\|^2_{L^2(\Omega_\mathrm{b})} + \frac{1}{2\Delta t}\|\sqrt{J}D_{n-1}\|^2_{L^2(\Omega_\mathrm{b})} + \|f(\theta_{\mathrm{b}_{n-1}})\,Y_{n-1}\,D_nJ\|_{L^1(\Omega_\mathrm{b})}, \tag{74}$$

$$\frac{1}{2\Delta t}\|\sqrt{J}D_n\|^2_{L^2(\Omega_\mathrm{b})} + \tilde{\beta}\|\sqrt{J}\nabla D_n\|^2_{L^2(\Omega_\mathrm{b})} \le \frac{1}{2\Delta t}\|\sqrt{J}D_{n-1}\|^2_{L^2(\Omega_\mathrm{b})} + \|f(\theta_{\mathrm{b}_{n-1}})\,Y_{n-1}\,D_nJ\|_{L^1(\Omega_\mathrm{b})}, \tag{75}$$

$$\frac{1}{2\Delta t}\|\sqrt{J}D_n\|^2_{L^2(\Omega_\mathrm{b})} \le \frac{1}{2\Delta t}\|\sqrt{J}D_{n-1}\|^2_{L^2(\Omega_\mathrm{b})} + \|f(\theta_{\mathrm{b}_{n-1}})\,Y_{n-1}\,D_nJ\|_{L^1(\Omega_\mathrm{b})}, \tag{76}$$

$$\frac{1}{2\Delta t}\|\sqrt{J}D_n\|^2_{L^2(\Omega_\mathrm{b})} \le \frac{1}{2\Delta t}\|\sqrt{J}D_{n-1}\|^2_{L^2(\Omega_\mathrm{b})} + \|\sqrt{J}f(\theta_{\mathrm{b}_{n-1}})\,Y_{n-1}\|_{L^2(\Omega_\mathrm{b})}\|\sqrt{J}D_n\|_{L^2(\Omega_\mathrm{b})}, \tag{77}$$

where the last inequality holds thanks to Holder's inequality. By summing over s we obtain

$$\sum_{s=1}^{n}\frac{1}{2\Delta t}\|\sqrt{J}D_s\|^2_{L^2(\Omega_\mathrm{b})} \le \frac{1}{2\Delta t}\sum_{s=1}^{n}\|\sqrt{J}D_{s-1}\|^2_{L^2(\Omega_\mathrm{b})} + \sum_{s=1}^{n}\|\sqrt{J}f(\theta_{\mathrm{b}_{s-1}})\,Y_{s-1}\|_{L^2(\Omega_\mathrm{b})}\|\sqrt{J}D_s\|_{L^2(\Omega_\mathrm{b})}, \tag{78}$$

$$\frac{1}{2\Delta t}\|\sqrt{J}D_n\|^2_{L^2(\Omega_\mathrm{b})} \le \frac{1}{2\Delta t}\|\sqrt{J}D_0\|^2_{L^2(\Omega_\mathrm{b})} + \sum_{s=1}^{n}\|\sqrt{J}f(\theta_{\mathrm{b}_{s-1}})\,Y_{s-1}\|_{L^2(\Omega_\mathrm{b})}\|\sqrt{J}D_s\|_{L^2(\Omega_\mathrm{b})} \tag{79}$$

$$\frac{1}{2\Delta t}\|\sqrt{J}D_n\|^2_{L^2(\Omega_\mathrm{b})} \le \frac{1}{2\Delta t}\|\sqrt{J}D_0\|^2_{L^2(\Omega_\mathrm{b})} + \sum_{s=1}^{n}\frac{1}{2}\|\sqrt{J}f(\theta_{\mathrm{b}_{s-1}})\,Y_{s-1}\|^2_{L^2(\Omega_\mathrm{b})} + \sum_{s=1}^{n}\frac{1}{2}\|\sqrt{J}D_s\|^2_{L^2(\Omega_\mathrm{b})}. \tag{80}$$

Now, Gronwall's Lemma assures us that

$$\|\sqrt{J}D_n\|^2_{L^2(\Omega_\mathrm{b})} \le C(t_n)\Big(\|\sqrt{J}D_0\|^2_{L^2(\Omega_\mathrm{b})} + \Delta t\sum_{s=1}^{n}\|\sqrt{J}f(\theta_{\mathrm{b}_{s-1}})\,Y_{s-1}\|^2_{L^2(\Omega_\mathrm{b})}\Big), \tag{81}$$

$$\Delta t\sum_{s=1}^{n}\|D_s^{(k)}\|^2_{L^2(\Omega_\mathrm{b})} \le M_{D_1}\tau\|D_0\|^2_{L^2(\Omega_\mathrm{b})} + M_{D_2}\tau^2\|Y_0\|^2_{L^2(\Omega_\mathrm{b})}. \tag{82}$$

Moreover, by summing over s the equation (75) we get

$$\frac{1}{2\Delta t}\|\sqrt{J}D_n\|^2_{L^2(\Omega_\mathrm{b})} + \sum_{s=1}^{n}\tilde{\beta}\|\sqrt{J}\nabla D_s\|^2_{L^2(\Omega_\mathrm{b})} \le \frac{1}{2\Delta t}\|\sqrt{J}D_0\|^2_{L^2(\Omega_\mathrm{b})} + \sum_{s=1}^{n}\frac{1}{2}\|\sqrt{J}f(\theta_{\mathrm{b}_{s-1}})\,Y_{s-1}\|^2_{L^2(\Omega_\mathrm{b})} + \sum_{s=1}^{n}\frac{1}{2}\|\sqrt{J}D_s\|^2_{L^2(\Omega_\mathrm{b})} \tag{83}$$

$$\Delta t\sum_{s=1}^{n}2\tilde{\beta}\|\sqrt{J}\nabla D_s\|^2_{L^2(\Omega_\mathrm{b})} \le \|\sqrt{J}D_0\|^2_{L^2(\Omega_\mathrm{b})} + \Delta t\sum_{s=1}^{n}\|\sqrt{J}f(\theta_{\mathrm{b}_{s-1}})\,Y_{s-1}\|^2_{L^2(\Omega_\mathrm{b})} + \Delta t\sum_{s=1}^{n}\|\sqrt{J}D_s\|^2_{L^2(\Omega_\mathrm{b})} \tag{84}$$

by substituting the above estimate for the last term, we obtain

$$\Delta t\sum_{s=1}^{n}\|\nabla D_s\|^2_{L^2(\Omega_\mathrm{b})} \le M_{D_3}\|D_0\|^2_{L^2(\Omega_\mathrm{b})} + M_{D_4}\tau\|Y_0\|^2_{L^2(\Omega_\mathrm{b})}. \tag{85}$$

We compute now the following estimate for $g_n^{(k)}$ when $\Delta t = \tau 2^{-k}$

$$\begin{aligned}
(86)\quad \Delta t \sum_{n=0}^{N(k)} \|g_n^{(k)}\|^2_{H(\Omega_\mathrm{b})} &= \Delta t \sum_{n=0}^{N(k)} \left[\|\theta_{\mathrm{b}_n}^{(k)}\|^2_{H^1(\Omega_\mathrm{b})} + \|D_n^{(k)}\|^2_{H^1(\Omega_\mathrm{b})} + \|Y_n^{(k)}\|^2_{L^2(\Omega_\mathrm{b})}\right] \\
&\leq M_{\mathrm{b}_1}\tau\|\theta_{\mathrm{b}_0}\|^2_{L^2(\Omega_\mathrm{b})} + M_{\mathrm{b}_2}\tau^2\,\|\theta_\mathrm{o}\|^2_{L^2(\partial\Omega_\mathrm{b})} + M_{b_3}\|\theta_{\mathrm{b}_0}\|^2_{L^2(\Omega_\mathrm{b})} + \tau\, M_{b_4}\|\theta_\mathrm{o}\|^2_{L^2(\partial\Omega_\mathrm{b})} + M_{D_1}\tau\|D_0\|^2_{L^2(\Omega_\mathrm{b})} \\
&\quad + M_{D_2}\tau^2\|Y_0\|_{L^2(\Omega_\mathrm{b})} + M_{D_3}\|D_0\|^2_{L^2(\Omega_\mathrm{b})} + M_{D_4}\tau\|Y_0\|^2_{L^2(\Omega_\mathrm{b})} + \tau\, c_Y\,\|Y_0\|^2_{L^2(\Omega_\mathrm{b})} =: c_1.
\end{aligned}$$

This estimate is uniform in k and leads to

$$(87)\quad \|g^{(k)}(\boldsymbol{X},t)\|^2_{L^2([0,\tau];H(\Omega_\mathrm{b}))} = \int_0^\tau \sum_{n=0}^{N(k)} \|g_n^{(k)}(\boldsymbol{X})\|^2_{H(\Omega_\mathrm{b})}\,\chi_{[t_n,t_n+\tau/2^k[}(t)\,dt = \sum_{n=0}^{N(k)} \Delta t\|g_n^{(k)}(\boldsymbol{X})\|^2_{H(\Omega_\mathrm{b})} \leq c_1.$$

This proves the boundedness which implies the weak convergence, up to the extraction of a sub-sequence, thanks to the reflexivity of $L^2([0,\tau];H(\Omega_\mathrm{b}))$.

D Convergence of the time derivative

Here we show how one can move the finite difference approximation of the time derivative from the unknown to the test function to justify equation (47). With $\Delta t = \tau/2^l$, we compute

(88)

$$\begin{aligned}
&\int_0^\tau \frac{\theta_\mathrm{b}^{(l)}(t) - \theta_\mathrm{b}^{(l)}(t-\Delta t)}{\Delta t}\tilde{g}(t)\,dt \\
&= \int_0^\tau \frac{\theta_\mathrm{b}^{(l)}(t)}{\Delta t}\tilde{g}(t)\,dt - \int_0^\tau \frac{\theta_\mathrm{b}^{(l)}(t-\Delta t)}{\Delta t}\tilde{g}(t)\,dt \\
&= \int_0^\tau \frac{\theta_\mathrm{b}^{(l)}(t)}{\Delta t}\tilde{g}(t)\,dt - \int_{-\Delta t}^{\tau-\Delta t} \frac{\theta_\mathrm{b}^{(l)}(t)}{\Delta t}\tilde{g}(t+\Delta t)\,dt \\
&= \int_0^{\tau-\Delta t} \frac{\theta_\mathrm{b}^{(l)}(t)}{\Delta t}\tilde{g}(t)\,dt + \int_{\tau-\Delta t}^\tau \frac{\theta_\mathrm{b}^{(l)}(t)}{\Delta t}\tilde{g}(t)\,dt - \int_{-\Delta t}^0 \frac{\theta_\mathrm{b}^{(l)}(t)}{\Delta t}\tilde{g}(t+\Delta t)\,dt - \int_0^{\tau-\Delta t} \frac{\theta_\mathrm{b}^{(l)}(t)}{\Delta t}\tilde{g}(t+\Delta t)\,dt \\
&= -\int_0^{\tau-\Delta t} \frac{\tilde{g}(t+\Delta t) - \tilde{g}(t)}{\Delta t}\theta_\mathrm{b}^{(l)}(t)\,dt + \int_{\tau-\Delta t}^\tau \frac{\theta_\mathrm{b}^{(l)}(t)}{\Delta t}\tilde{g}(t)\,dt - \int_{-\Delta t}^0 \frac{\theta_\mathrm{b}^{(l)}(t)}{\Delta t}\tilde{g}(t+\Delta t)\,dt.
\end{aligned}$$

Taking now the limit $l \to \infty$, which gives also $\Delta t \to 0$, on both ends of the previous chain of identities, we obtain

$$(89)\qquad \int_0^\tau \frac{\partial\bar{\theta}_\mathrm{b}(t)}{\partial t}\tilde{g}(t)\,dt = -\int_0^\tau \frac{\partial\tilde{g}(t)}{\partial t}\bar{\theta}_\mathrm{b}(t)\,dt + \tilde{g}(\tau)\bar{\theta}_\mathrm{b}(\tau) - \tilde{g}(0)\bar{\theta}_\mathrm{b}(0).$$

References

1. J. Paton, Z. Khatir, H. Thompson, N. Kapur, and V. Toropov, Thermal energy management in the bread baking industry using a system modelling approach, *Applied Thermal Engineering*, vol. 53, issue 2, pp. 340–347, 2013.
2. M. Al-Nasser, I. Fayssal, and F. Moukalled, Numerical simulation of bread baking in a convection oven, *Applied Thermal Engineering*, vol. 184, p. 116252, 2021.
3. F. H. Pask, J. Sadhukhan, P. Lake, S. McKenna, E. B. Perez, and A. Yang, Systematic approach to optimize industrial ovens for energy saving, *21st International Congress of Chemical and Process Engineering, CHISA 2014 and 17th Conference on Process Integration, Modelling and Optimisation for Energy Saving and Pollution Reduction, PRES 2014*, vol. 4, no. 1, p. 2252, 2014.

4. E. Purlis, Bread baking: Technological considerations based on process modelling and simulation, *Journal of Food Engineering*, vol. 103, issue 1, pp. 92–102, 2011.
5. E. Purlis, Baking process design based on modelling and simulation: Towards optimization of bread baking, *Food Control*, vol. 27, issue 1, pp. 45–52, 2012.
6. B. Zanoni, C. Peri, and S. Pierucci, A study of the bread-baking process. I: A phenomenological model, *Journal of Food Engineering*, vol. 19, issue 4, pp. 389–398, 1993.
7. S. R. Ravula, D. Arepally, and A. K. Datta, Estimation of the energy requirement of bread during baking by inverse heat transfer method, *Journal of Thermal Analysis and Calorimetry*, vol. 148, issue 23, pp. 13297–13311, 2023.
8. J. Zhang and A. K. Datta, Mathematical modeling of bread baking process, *Journal of Food Engineering*, vol. 75, issue 1, pp. 78–89, 2006.
9. A. Romano, G. Toraldo, S. Cavella, and P. Masi, Description of leavening of bread dough with mathematical modelling, *Journal of Food Engineering*, vol. 83, issue 2, pp. 142–148, 2007.
10. P. P. Packkia-Doss, S. Chevallier, A. Pare, and A. Le-Bail, Effect of supplementation of wheat bran on dough aeration and final bread volume, *Journal of Food Engineering*, vol. 252, pp. 28–35, 2019.
11. E. Chiotellis and G. M. Campbell, Proving of bread dough II: Measurement of gas production and retention, *Food and Bioproducts Processing: Transactions of the Institution of Chemical Engineers, Part C*, vol. 81, issue 3, pp. 207–216, 2003.
12. B. de Cindio and S. Correra, Mathematical modelling of leavened cereal goods, *Journal of Food Engineering*, vol. 24, issue 3, pp. 379–403, 1995.
13. P. Shah, G. M. Campbell, S. L. Mckee, and C. D. Rielly, Proving of bread dough: Modelling the growth of individual bubbles, *Food and Bioproducts Processing: Transactions of the Institution of Chemical Engineers, Part C*, vol. 76, issue 2, pp. 73–79, 1998.
14. L. Rinaldi, E. Chinellato, P. Martin, and F. Marcuzzi, Exploiting Scientific Machine Learning on Embedded Digital Twins, in *Emerging Technologies in Computational Sciences for Industry, Sustainability and Innovation – Math to Product*, ed. by M. Giacomini, S. Perotto, and G. Rozza, vol. 146 of *Lecture Notes in Computational Science and Engineering*, Cham: Springer, 2025.
15. C. Krupitzer, T. Noack, and C. Borsum, Digital food twins combining data science and food science: system model, applications, and challenges, *Processes*, vol. 10, no. 9, p. 1781, 2022.
16. F. Erdogdu, Mathematical modeling of food thermal processing: Current and future challenges, *Current Opinion in Food Science*, vol. 51, p. 101042, 2023.
17. M. Kannapinn, M. K. Pham, and M. Schäfer, Physics-based digital twins for autonomous thermal food processing: Efficient, non-intrusive reduced-order modeling, *Innovative Food Science & Emerging Technologies*, vol. 81, p. 103143, 2022.
18. P. Verboven, T. Defraeye, A. K. Datta, and B. Nicolai, Digital twins of food process operations: the next step for food process models?, *Current Opinion in Food Science*, vol. 35, pp. 79–87, 2020.
19. M. E. Gurtin, *An introduction to Continuum Mechanics*, vol. 158 of *Mathematics in Science and Engineering*, New York: Academic Press, 1981.
20. A. Quarteroni, *Numerical Models for Differential Problems*, 2nd edition, vol. 8 of *Modeling, Simulation and Applications*, Milano: Springer, 2014.
21. S. Chevallier, R. Zúñiga, and A. Le-Bail, Assessment of bread dough expansion during fermentation, *Food and Bioprocess Technology*, vol. 5, issue 2, pp. 609–617, 2012.
22. M. Stanke, V. Zettel, S. Schütze, and B. Hitzmann, Measurement and mathematical modeling of the relative volume of wheat dough during proofing, *Journal of Food Engineering*, vol. 131, pp. 58–64, 2014.
23. E. Chinellato, F. Marcuzzi, and S. Pierobon, Physics-Aware Soft Sensors for Embedded Digital Twins, in *Proceedings of Ninth International Congress on Information and Communication Technology*, ed. by X.-S. Yang, S. Sherratt, N. Dey, and Joshi A., vol. 1013 of *Lecture Notes in Networks and Systems*, Singapore: Springer, 2024, pp. 417–427.